AGU PUBLICATIONS

JGR

Journal of Geophysical Research: Oceans

RESEARCH ARTICLE

10.1002/2015JC011400

Data and numerical analysis of astronomic tides, wind-waves, and hurricane storm surge along the northern Gulf of Mexico

M. V. Bilskie[1], S. C. Hagen[1,2], S. C. Medeiros[3], A. T. Cox[4], M. Salisbury[5], and D. Coggin[6]

[1]Department of Civil and Environmental Engineering, Louisiana State University, Baton Rouge, Louisiana, USA, [2]Center for Computation and Technology, Louisiana State University, Baton Rouge, Louisiana, USA, [3]Department of Civil, Environmental and Construction Engineering, University of Central Florida, Orlando, Florida, USA, [4]Oceanweather Inc., Cos Cob, Connecticut, USA, [5]Atkins Global, Melbourne, Florida, USA, [6]Marea Technology, Green Cove Springs, Florida, USA

Key Points:
- A numerical storm surge model was developed using the most recent and publicly available data
- Observed data and numerical analysis explain the major surge generating mechanisms
- The Gulf of Mexico continental shelf contributes to hurricane-forced sea level anomalies

Supporting Information:
- Supporting Information S1
- Supporting Information S2
- Data Set S1
- Data Set S2
- Data Set S3
- Data Set S4
- Data Set S5
- Data Set S6
- Data Set S7
- Data Set S8
- Movie S1
- Movie S2
- Movie S3
- Movie S4

Correspondence to:
M. V. Bilskie,
Matt.Bilskie@gmail.com

Citation:
Bilskie, M. V., S. C. Hagen, S. C. Medeiros, A. T. Cox, M. Salisbury, and D. Coggin (2016), Data and numerical analysis of astronomic tides, wind-waves, and hurricane storm surge along the northern Gulf of Mexico, *J. Geophys. Res. Oceans*, *121*, 3625–3658, doi:10.1002/2015JC011400.

Received 16 OCT 2015
Accepted 20 APR 2016
Accepted article online 26 APR 2016
Published online 30 MAY 2016

Abstract The northern Gulf of Mexico (NGOM) is a unique geophysical setting for complex tropical storm-induced hydrodynamic processes that occur across a variety of spatial and temporal scales. Each hurricane includes its own distinctive characteristics and can cause unique and devastating storm surge when it strikes within the intricate geometric setting of the NGOM. While a number of studies have explored hurricane storm surge in the NGOM, few have attempted to describe storm surge and coastal inundation using observed data in conjunction with a single large-domain high-resolution numerical model. To better understand the oceanic and nearshore response to these tropical cyclones, we provide a detailed assessment, based on field measurements and numerical simulation, of the evolution of wind waves, water levels, and currents for Hurricanes Ivan (2004), Dennis (2005), Katrina (2005), and Isaac (2012), with focus on Mississippi, Alabama, and the Florida Panhandle coasts. The developed *NGOM3* computational model describes the hydraulic connectivity among the various inlet and bay systems, Gulf Intracoastal Waterway, coastal rivers and adjacent marsh, and built infrastructure along the coastal floodplain. The outcome is a better understanding of the storm surge generating mechanisms and interactions among hurricane characteristics and the NGOM's geophysical configuration. The numerical analysis and observed data explain the ~2 m/s hurricane-induced geostrophic currents across the continental shelf, a 6 m/s outflow current during Ivan, the hurricane-induced coastal Kelvin wave along the shelf, and for the first time a wealth of measured data and a detailed numerical simulation was performed and was presented for Isaac.

1. Introduction

The Gulf of Mexico (GoM) is one of the few seas that is both partially landlocked and adjacent to an open ocean. The basin is almost entirely enclosed by a broad and shallow continental shelf (less than 180 m deep) representing 22% of the entire basin area [*Gore*, 1992]. Along the eastern GoM, the wide and gently sloping West Florida Shelf (WFS) extends from the Florida Keys to the Florida Panhandle, and the Mississippi-Alabama (MS-AL) Shelf ranges from the Florida Panhandle to the Mississippi River Delta (Figure 1a). The shelf provides a buffer between the deep ocean and the shallow coastal zone. However, the wide shelf also contributes to local- and deep-water forced sea level anomalies. Tropical cyclone induced sea level surges are generated from the complex geography of the GoM and cause wide-spread flooding in low-lying regions [*Kennedy et al*., 2011; *Morey et al*., 2006; *Weisberg and He*, 2003].

In the nearshore, the northern Gulf of Mexico (NGOM) [defined herein as spanning the Mississippi, Alabama, and Florida Panhandle coasts] contains a vast expanse of barrier islands, stretches of intertidal salt marsh adjacent to numerous coastal rivers, and an abundance of inlet and bay systems connected via the Gulf Intracoastal Waterway (GIWW). The NGOM's geophysical settings drive complex hydrodynamic processes that vary broadly through shelf- and local-scale circulation. The NGOM also possesses a diverse history of recent tropical storm activity, including Hurricanes Ivan (2004), Dennis (2005), Katrina (2005), and Isaac (2012) (Figure 1a), with each hurricane and accompanying surge well documented (National Oceanic and Atmospheric Administration [NOAA] National Hurricane Center, http://www.nhc.noaa.gov/data/). Each event possesses its own unique and inherent characteristics, and can cause remarkable storm surge when

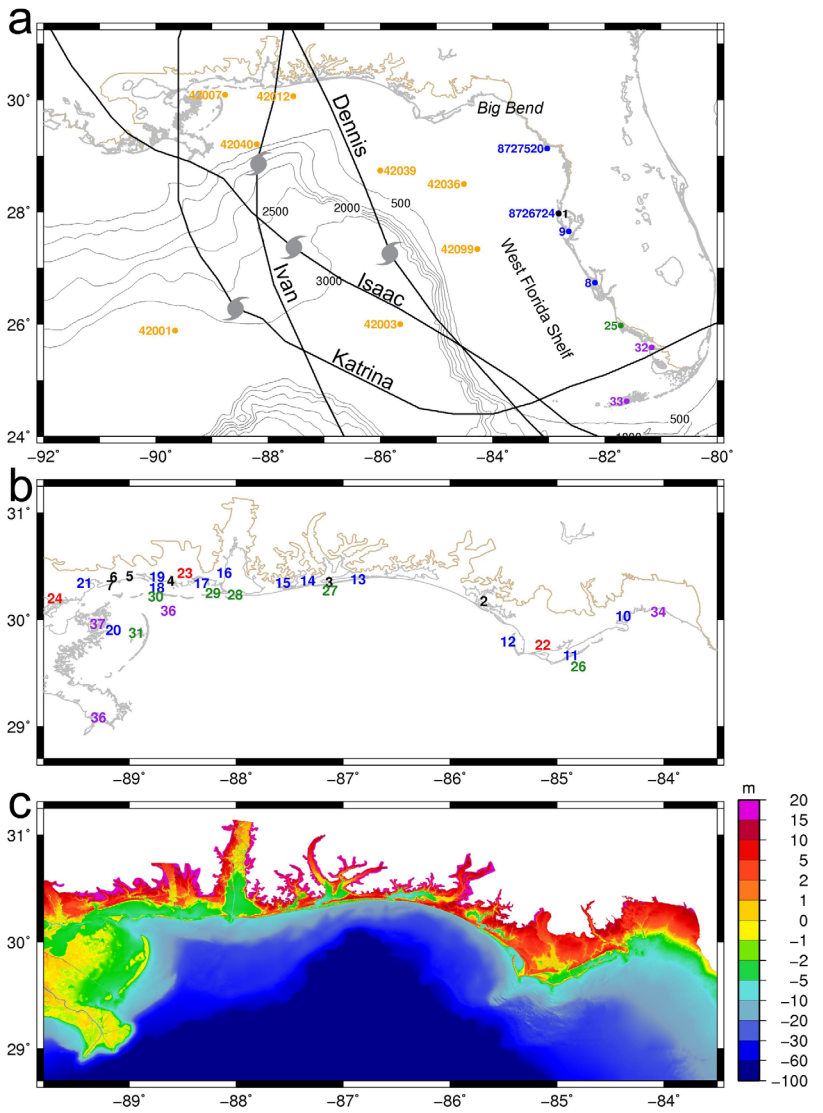

Figure 1. (a) Location map of the Gulf of Mexico. NDBC buoys locations are in orange, two NOAA stations located outside the NGOM nearshore region are in blue, and significant coastal features are shown as in Table 1. Tracks for Hurricane Ivan, Dennis, Katrina, and Isaac are shown in black. Bathymetric contours (as labeled) are shown as thin black lines, the coastline in grey, and *NGOM3* inland boundary in tan. (b) Locations of interest along the NGOM; cities (black), water bodies (blue), rivers (red), island (green), and places and features (purple) as shown in Table 1. (c) *NGOM3* model elevations (m, NAVD88).

combined with the geometric and topographical characteristics of the GoM. In order to mitigate the damage and displacement from future coastal disasters, it is important to understand the evolution of storm surge and wind-waves from the deep ocean, onto the wide and broad continental shelf, into the nearshore and across the coastal landscape [*Resio and Westerink*, 2008]. These recent storms, the wealth of available data and our ability to perform high-resolution numerical assessments provide us an opportunity to understand the distinct responses to a wide range of extreme activity in the NGOM.

There are numerous physics-based numerical models developed for simulating astronomic tides and hurricane storm surge. Each employ their own numerical discretization scheme, spatial and temporal resolution, and model boundary and forcing mechanisms [*Bunya et al.*, 2010; *Chen et al.*, 2008; *Dietrich et al.*, 2011b; *Ding et al.*, 2013; *Dukhovskoy and Morey*, 2011; *Hope et al.*, 2013; *Kennedy et al.*, 2011; *Sheng et al.*, 2010; *Weisberg and Zheng*, 2008; *Yang et al.*, 2014]. In particular, a suite of southern Louisiana (SL) and Texas ADCIRC [*Luettich et al.*, 1992] models have been extensively refined over the past decade and have set the precedent in hurricane storm surge hindcasting studies [*Hope et al.*, 2013].

Table 1. Identification of Geographic Locations as Shown in Figure 1

Cities	
1	Clearwater
2	Panama City
3	Pensacola
4	Pascagoula
5	Biloxi
6	Gulfport
7	Pass Christian
Bays and Sounds	
8	Charlotte Harbor
9	Tampa Bay
10	Apalachee Bay
11	Aplachicola Bay
12	St. Joseph Bay
13	Santa Rosa Sound
14	Pensacola Bay
15	Perdido Bay
16	Mobile Bay
17	Grand Bay
18	Mississippi Sound
19	Biloxi Bay
20	Chandeleur Sound
21	Bay of St. Louis
Rivers	
22	Apalachicola River
23	Pascagoula River
24	Pearl River
Islands	
25	Marco Island
26	St. George Island
27	Santa Rosa Island
28	Fort Morgan Penninsula
29	Dauphin Island
30	Mississippi Barrier Islands
31	Chandeleur Island
Places and Features	
32	Everglades
33	Florida Keys
34	Shell Point
35	MSAL Shelf
36	LA Birds Foot
37	Biloxi Marsh

Yang et al. [2014] developed an FVCOM (Finite Volume Coastal Ocean Model) [*Chen et al.*, 2003] model to simulate tides and storm surge from Hurricanes Rita, Katrina, Ivan, and Dolly. They validated against NOAA stations for tides and surge, but the focus was on examining coastal inundation due to surge, SLR, and subsidence, particularly in the Louisiana marsh. They report good model agreement with measured data but mention that results could improve with finer model resolution.

A few studies have focused on Hurricane Ivan, but with little emphasis on model validation, especially in regions outside of Pensacola Bay. *Salisbury and Hagen* [2007] examined the role of tidal inlet systems on open coast storm surge hydrographs using a Hurricane Ivan forced numerical model within Pensacola Bay as a real-world case study. *Hagen et al.* [2011] studied the sensitivity of wind drag coefficients and its implications on maximum water surface elevations for the four hurricanes that struck Florida's coast in 2004 (Hurricanes Charley, Frances, Jeanne, and Ivan). *Sheng et al.* [2010] employed the coupled CH3D-SWAN model to the northeastern GoM to simulate hydrodynamics of Hurricane Ivan and state the importance of including land dissipation on hurricane winds, and they also conducted experiments between 2D and 3D model formulations. *Chen et al.* [2008] developed a coarse ADCIRC model with loose coupling to SWAN of the NGOM to study Hurricanes Ivan and Katrina. The model was designed to run on a personal workstation, not a high-performance computer. The objective was to quantify the hydrodynamic response in the NGOM and better understand the factors that control the dynamic nature of storm surge and wind waves in a shallow coastal region. Although not the emphasis, model validation was focused on the Mobile and Pensacola Bay regions and did not include an analysis of high water marks (HWM).

Studies involving Hurricane Dennis were focused on the classification and generation of the remotely generated sea level anomaly and its contribution to the maximum storm tide in the Big Bend region of Florida [*Dukhovskoy and Morey*, 2011; *Morey et al.*, 2006]. *Morey et al.* [2006] demonstrated the need for larger model domains in order to accurately capture remotely generated shelf waves. They showed, through numerical modeling, that Hurricane Dennis induced surges of 1.8 m (NAVD88) above the predicted tide in a region 275 km east of the landfall location. *Dukhovskoy and Morey* [2011] continued that work by simulating Hurricane Dennis with a higher resolution mesh (25 to 100 m) and compared model results among 2D and 3D FVCOM simulations. The Apalachee FVCOM model was nested into the GoM model from *Morey et al.* [2006] and was forced only with winds. These previous assessments were focused on understanding the remotely forced sea level rise during Hurricane Dennis and comparison of 2D and 3D results; however, the full physics of the event were not simulated and fully evaluated. For example, *Dukhovskoy and Morey* [2011] did not directly include model forcing from astronomic tides, pressure, or wind generated waves, and only

simulated storm surge based on wind stress. These effects were added *post festum* using empirical and theoretical methods. Additionally, estimates of storm surge were only compared to measured data at Shell Point (NDBC SHPF1) and at six tide gauges, and a limited HWM error analysis was performed. Furthermore, it was not definitively illustrated that the 3D model better fits the 2D result in terms of the full surge hydrograph (peak surge, timing of the peak, and surge volume).

In addition, each of these models, among many others, were designed and developed with an individual storm event in mind. When constructing storm surge models for real-time forecasting or analysis of future conditions (such as climate change in general and sea level rise in particular), these models must be able to accurately simulate multiple events without additional model calibration [*Bilskie et al*., 2014; *Resio and Westerink*, 2008]. There are studies concerning model validation for multiple storm events that span many years employing the same model setup; the only published work found in recent literature was *Dietrich et al*. [2012] and *Yang et al*. [2014]. Moreover, with respect to storm surge hindcasting studies, there is a gap in published literature for Hurricanes Ivan (2004), Dennis (2005), and Isaac (2012); Hurricane Katrina has been extensively studied, but attention has been on southern Louisiana without particular focus on the Mississippi, Alabama, and Florida regions. In this paper, we fill this gap, and provide a detailed assessment from data and numerical simulations, including the validation of our model, and the evolution of wind-waves, water levels and currents for Hurricanes Ivan, Dennis, Katrina, and Isaac, with focus on Mississippi, Alabama, and the Florida Panhandle coasts (Figure 1b). While doing so, we introduce a high-resolution storm surge model for the NGOM, named *NGOM3*.

The *NGOM3* model captures the essential circulation interactions among the deep-water, continental shelf, and nearshore regions and provides inland hydraulic connectivity through the GIWW. The most recent publically available data were used in order to produce a model representative of the year c. 2012. We first validate the model against observed astronomic tides. The validation of tides demonstrates the model resolves important coastal features (in the deep water and nearshore) in terms of spatial discretization, accurate bathymetry, and accurate dissipation via bottom friction. We then examine the large-scale, regional, and local circulation patterns within the GoM and compare model results to measured waves and water levels from four historical hurricanes: Ivan, Dennis, Katrina, and Isaac. Each of the four storm surge simulations uses the exact same model setup (model mesh and surface roughness characteristics), with the only modification being the meteorological and astronomic tide forcing.

The paper is presented as follows: First, the numerical code is presented and followed by a description of data sources used, unstructured mesh generation, derivation of surface roughness parameters, and model forcing. The *NGOM3* model is setup to simulate astronomic tides only, and results are compared to measured data across the study domain. Next, a hindcast for Hurricanes Ivan, Dennis, Katrina, and Isaac are presented. The evolution of hurricane-induced winds, waves, currents, and water levels are described, and model results are compared to a variety of recorded wave, current, and water level data.

2. Methods

2.1. Wave and Surge Model

The barotropic two-dimensional, unstructured finite element code ADCIRC (Advanced Circulation) was implemented to compute depth-averaged water surface elevations and currents in the x and y directions using the modified shallow water equations [*Kolar et al*., 1994; *Luettich and Westerink*, 2004]. The 2D depth-averaged equations are applicable due to the strong wave-induced vertical mixing across the continental shelf during a hurricane event [*Dietrich et al*., 2011b; *Hope et al*., 2013]. Vertical mixing during the passage of a hurricane was displayed in the reduced sea surface temperature (SST) in the wake of the storm, as observed during Hurricane Dennis (2005). Strong vertical mixing allowed sediment resuspension across the WFS in depths less than 50 m [*Hu and Muller-Karger*, 2007]. Measurements at 14 acoustic Doppler current profilers deployed near the path of Hurricane Ivan showed strong wave-induced near-bottom currents at a depth of 60 m, indicating a well-mixed vertical layer up to 60 m water depth [*Mitchell et al*., 2005; *Teague et al*., 2007]. A turbulence resolving large-eddy simulation of Hurricane Frances (2004) indicated that the upper ocean boundary layer reaches a depth of 100 m due to the synergy of the winds, waves and currents [*Hope et al*., 2013; *Sullivan et al*., 2012].

ADCIRC is coupled to the third generation wave model, SWAN, which solves the action balance equation for relative frequency and wave direction, and each model uses the same unstructured mesh [*Booij et al*., 1999; *Dietrich et al*., 2011a, 2012; *Holthuijsen*, 2007; *Zijlema*, 2010]. In this study, ADCIRC was run with a 1.0 s time step, solving for water levels and currents, which were passed to SWAN every 600 s (the SWAN time step). After obtaining information from ADCIRC, SWAN computed wave radiation stress gradients and passed them to ADCIRC. SWAN simulated wave frequencies and directions were discretized into 40 frequency bins and 36 bins of 10°, respectively. Wind-induced wave growth was based on *Komen et al*. [1984] and *Cavaleri and Rizzoli* [1981], modified whitecapping from *Rogers et al*. [2003], *Battjes and Janssen* [1978] depth-induced wave breaking with wave breaking index equal to 0.73, and bottom roughness via Manning's *n* was passed from ADCIRC using *Madsen et al*. [1988] roughness length formulation. False wave refraction was limited in regions of inadequate mesh resolution using a spectral propagation velocity limiter [*Dietrich et al*., 2013].

2.2. *NGOM3* Unstructured Mesh

Simulations were performed using the SWAN+ADCIRC numerical code and framework on the *NGOM3* computational mesh. The *NGOM3* mesh is the spatial discretization to which state variables and material types are mapped for inputs and outputs. The mesh spans the western North Atlantic Ocean, Caribbean Sea, and GoM and describes the inland region up to the 15 m (NAVD88) land elevation contour from southeastern Louisiana to Florida's Big Bend region (west to east). The 5.5 million node *NGOM3* mesh is an experiential product of the development of three previous meshes, *MSAL* (Mississippi-Alabama) [*Bilskie et al*., 2015], *FLPH_AL* (Florida Panhandle and Alabama) [*University of Central Florida*, 2011b], and *FWJ* (Franklin, Wakulla, and Jefferson Counties, FL) [*Hagen et al*., 2009; *Salisbury et al*., 2011] and employs mesh generation techniques that have been established over the last 15 years [*Hagen and Parrish*, 2004; *Hagen et al*., 2000, 2001]. Since the intricate details on the mesh generation process are presented in *Bilskie et al*. [2015], we focus the description herein on the data employed with minimal discussion on the meshing.

2.2.1. Bathymetric and Topographic Data Sources

The shoreline was defined based on manual digitization according to present day aerial imagery. The shoreline serves as the interface between topographic and bathymetric data sets (zero elevation NAVD88 contour). The bathymetry consists of 17 separate data sets that were constructed from a variety of sources, with the objective of describing the bathymetry with the best available and most accurate data. The bathymetric data sources used in the construction of the bathymetric elevation model were obtained from (in order of importance or extent of study area): National Ocean Service (NOS) Hydrographic Surveys (http://www.ngdc.noaa.gov/mgg/bathymetry/hydro.html), US Army Corps of Engineers (USACE) Channel Surveys, Apalachicola River cross sections, Pascagoula River cross sections, NOAA Nautical Charts, Northwest Florida Water Management District (NWFWMD) boat-mounted, GPS-enabled, depth sounder surveys, and field knowledge. Since all of the bathymetric data were aligned to a variety of vertical tidal and geodetic datums, all were converted to reference NAVD88. Conversion to the NAVD88 datum was done using NOAA's VDatum tool (http://vdatum.noaa.gov/welcome.html). In regions outside the VDatum coverage area, tide gauges and nearby VDatum conversion values were used [*Medeiros et al*., 2011]. The Apalachicola River cross sections were converted from NGVD29 to NAVD88 using the CorpsCon software (http://www.agc.army.mil/Missions/Corpscon.aspx). In preparation for the generation of a bathymetric triangular irregular network, numerous constraint lines (breaklines) were added to impose bathymetric contours and flow lines. Using these interior constraints, along with the shoreline as a boundary, all bathymetric data were triangulated to generate a bathymetric data set [*Bilskie et al*., 2015; *Coggin et al*., 2011; *University of Central Florida*, 2011a]

The coastal landscape in the study area was mainly covered by recent lidar data. All state-wide data for Florida and Alabama were provided by the Northwest Florida Water Management District (NWFWMD). Lidar data in Mississippi were obtained via NOAA Digital Coast, Coastal Topographic Lidar (http://coast.noaa.gov/digitalcoast/). Additional lidar data were obtained from the NASA Experimental Advanced Airborne Research Lidar (EAARL) system and Joint Airborne Lidar Bathymetry Technical Center of Expertise (JALBTCX) CHARTS system. The USGS National Elevation Dataset (NED) was used to supplement in the Mobile-Tensaw Delta area, north of Mobile and Baldwin Counties, AL, due to lack of lidar. Topographic elevations outside the study region in Louisiana were obtained from the SL18 storm surge model [*Dietrich et al*., 2011b]. Along with hydrographic breaklines and the digitized shoreline, the bare earth lidar was interpolated via natural neighbor interpolation to a 5 m resolution digital elevation model (DEM).

2.2.2. Vertical Feature Delineation

Natural and manmade vertical features were extracted using the methods presented in *Bilskie et al*. [2015]. Typical features include raised roadbeds, coastal dunes, natural ridges and valleys, and small rivers and tidal creeks. These features were extracted in order to precisely locate features that may alter the path, pattern, and magnitude of surge propagation, by inhibiting or promoting flow [*University of Central Florida*, 2011a]. The extracted vertical lines were used as interior constraints during the mesh generation process whereby element edges were aligned to the feature lines.

2.2.3. Unstructured Mesh

The numerical mesh was developed, first and foremost, to resolve coastal waterway features such as bays and inlets, the Gulf Intracoastal Waterway, dredged channels, coastal rivers, and tidal creeks. These features were resolved using, at least, three unstructured elements across the channel. Minimum model resolution criteria was set to 15–20 m, based on the Courant-Friedrichs-Lewy condition to achieve a 1 s time step in ADCIRC; therefore, inland waterways that were at least 60 m in width were generally discretized with sufficient resolution to model the channel with a trapezoidal cross section. Using the manually digitized shoreline as the boundary, an in-bank mesh was developed in order to enforce appropriate hydraulic connectivity among the various inland waterways.

The final *NGOM3* mesh includes 5,492,546 nodes and 10,945,358 elements. Mesh resolution ranges from 25 km in the deep Atlantic Ocean, 4 km in the deep GoM, 1 km along the continental shelf, 100–200 m along the shoreline and wave breaking zones, and down to 15–20 m in small inland waterways. The large domain allows the model to capture the evolution of wind-generated waves and hurricane storm surge across a variety of spatial and temporal scales.

2.2.4. Surface Roughness

ADCIRC incorporates three surface roughness parameters to account for bottom friction, canopy, and wind reduction. ADCIRC uses spatially varying Manning's n coefficients for hydraulic bottom friction parameterization. Over the floodplain, Manning's n is based on the post-Katrina Coastal Change Analysis Program (C-CAP) (http://www.csc.noaa.gov/digitalcoast/data/ccapregional/) land use land cover (LULC) data set. Manning's n for each LULC classification were interpolated onto the mesh using direct lookup to account for sharp discontinuities in LULC type [*Bilskie et al*., 2015; *Dietrich et al*., 2011b]. *Weisberg and Zheng* [2008] point out that bottom stress parameterization across the shelf and deep ocean should reflect bottom sediment type. *Kennedy et al*. [2011] confirmed this and subsequently found that properly assigning bottom friction based on sediment type leads to improved results when computing Hurricane Ike's forerunner using the barotropic ADCIRC model. The method set forth by *Kennedy et al*. [2011] and *Martyr et al*. [2013] was applied across the Louisiana-Texas shelf and continued across the WFS. In the nearshore and deep ocean, Manning's n is derived from bottom sediment type and the local depth [*Buczkowski et al*., 2006]. Across the WFS and in depths less than 5 m, Manning's n was assigned to 0.022 for coarse sediments (sand/gravel) and across the Mississippi and Alabama shelf Manning's n was 0.012 to represent finer sediments (mud). In the deep Gulf (depths greater than 200 m) Manning's n was assigned to 0.012. Manning's n in depths between 5 m and the shoreline (0 m) are was linearly interpolated from the local value to 0.025 [*Dietrich et al*., 2012; *Hope et al*., 2013; *Martyr et al*., 2013]. Back bays were assigned values of 0.022 and coastal rivers were assigned a Manning's n value of 0.022–0.035, depending on their depth and sinuosity [*Chow*, 1959].

Similarly, canopy and wind reduction factors were assigned based on the CCAP land cover database. Canopy values are either 0 or 1, meaning there is (0) or is not (1) sufficient canopy to block wind stress against the water surface. The anisotropic surface roughness (z_0) values reduce wind speed at a location based on up-wind conditions. This is extremely critical when hurricane winds interact with drastic changes from open water conditions to land. ADCIRC uses z_0 to adjust the wind speed at each node based on wind direction every 30 compass degrees instantaneously during runtime [*Atkinson et al*., 2011; *Bilskie et al*., 2015].

2.3. Astronomic Tide Forcing

The eight dominant astronomic tides (O1, K1, P1, Q1, M2, S2, N2, and K2) were applied along the open ocean boundary (60° west Meridian) where tidal amplitudes and phases are well known, and were derived from Oregon State's TPXO7.2 tidal atlas [*Egbert and Erofeeva*, 2002; *Egbert et al*., 1994]. Tidal potential forcing was included in the interior of the domain using the same eight tidal constituents [*Luettich and Westerink*, 2000]. For the astronomic tide validation, the simulation began with a cold start and was hyperbolically ramped for 20 days, followed by 25 days of dynamic steady state, and harmonics were analyzed during the last 60 days. For the hurricane hindcast simulations, tides were adjusted based on nodal factors and equilibrium arguments.

2.4. Meteorological Forcing

Wind and pressure fields for each of the four hurricanes were developed using a blend of objectively analyzed measurements and modeled winds and pressures as described in *Bunya et al.* [2010]. The wind and pressure fields for Hurricane Ivan, Dennis, and Katrina were developed using NOAA's H*WIND (Hurricane Research Division Wind Analysis System) for the inner core [*Powell et al.*, 1998] and blended with Gulf-scale winds from the IOKA (Interactive Objective Kinematic Analysis) system [*Cox et al.*, 1995]. The resulting wind field applied to the ADCIRC model is 10 m height marine exposed wind speed at 15 min intervals. This study applied the same Katrina inputs as *Bunya et al.* [2010], which used an H*Wind [*Powell et al.*, 2010] reanalysis in the core of the system. While the analysis of Isaac (2012) referenced the H*Wind data, the core of the storm was modeled using the latest version of the TC96 mesoscale model [*Thompson and Cardone*, 1996]. The final set of marine based wind fields are 30 min sustained wind speeds at a height of 10 m. The wind and pressure field has a resolution of 0.1° for the GoM basin and a finer resolution of 0.025° across the regional northern GoM domain. Wind drag coefficients were applied based on storm sectors, derived from the location and translation direction of the hurricane. In sectors with counter directional wind and waves, the wind stress was greater than when the wind and waves align in similar directions. The use of directional wind stress based on storm sector has been shown to include additional physical mechanisms between the atmospheric and oceanic boundaries and improve storm surge model results based on archaic wind stress formulations [*Black et al.*, 2007; *Dietrich et al.*, 2011b; *Garratt*, 1977; *Powell*, 2006; *Powell et al.*, 2003]. The approach to developing the tropical wind and pressure fields have been documented and verified in numerous ocean response studies [*Bacopoulos et al.*, 2012; *Bunya et al.*, 2010; *Dietrich et al.*, 2011b; *Hope et al.*, 2013].

2.5. Quantitative Error Metric Analysis

Measured and simulated tidal constituents were compared via a tidal resynthesis for the first spring-neap cycle of a tidal epoch (~14.7 days) at 43 tidal gauges along the Florida Panhandle, Alabama, and Mississippi coast (supporting information File S1). Simulated water surface elevations were analyzed over 60 days and tidal constituent amplitudes and phases for 23 tidal constituents were computed. At each gauge, two error metrics were used for a quantitative analysis. The first measure is the mean squared error (MSE) divided by the population variance (VAR) of the observed data [*Bacopoulos et al.*, 2011]:

$$\frac{MSE}{VAR} = \frac{\sum_t (O_t - S_t)^2}{\sum_t (O_t - \bar{O})^2} \tag{1}$$

where O_t is the observed value, S_t is the simulated value, $\bar{O}$ is the mean of the observed values, and the summation of time t is every 60 s to 14.75 days. The second error measure is the root mean square error (RMSE):

$$RMSE = \sqrt{\frac{1}{N}\sum_t (O_t - S_t)^2} \tag{2}$$

where N is the number of data points for comparison.

For each hurricane event an assessment between observed and simulated water surface elevations was performed using quantitative measures of scatter index (SI):

$$SI = \frac{\sqrt{\frac{1}{n}\sum_{i=1}^{N} (S_i - O_i)^2}}{\frac{1}{n}\sum_{i=1}^{N} O_i} \tag{3}$$

and relative bias:

$$Relative\ Bias = \frac{\frac{1}{N}\sum_{i=1}^{N} (S_i - O_i)}{\frac{1}{N}\sum_{i=1}^{N} O_i} \tag{4}$$

where N is the total number of data points. SI and relative bias are common methods to qualitatively compare measured and recorded time-series water levels [*Hope et al.*, 2013]. Stations that had water level

influence from river runoff or included erroneous data, such as unknown datums, were withheld from the statistical analysis.

Poststorm collected HWMs were also used to validate the simulated peak storm tide. The full set of HWMs were first examined for accuracy to identify measurements that included effects from wave setup and runup, and other anomalies such as river runoff [*Luther et al*., 2007]. HWMs that contained errors, wave or river effects, or other anomalies were discarded. Additionally, HWMs that contained simulated errors residing outside of the interquartile range (IQR) were discarded:

$$\begin{aligned} E_i &< Q_1 + 1.5 * IQR \\ E_i &> Q_3 + 1.5 * IQR \end{aligned} \tag{5}$$

where Q_1 and Q_3 are the first and third quartiles, $IQR = Q_3 - Q_1$, the error at HWM i is $E_i = S_i - O_i$, between the simulated, S_i, and observed, O_i, values. This is a typical outlier removal method in the context of HWMs and gauge peaks [*Bunya et al*., 2010; *Dietrich et al*., 2011b].

3. Results and Discussion

The simulated oceanic and nearshore response to astronomic tides and meteorological forcing is presented as follows. First, *NGOM3* simulated astronomic tides are presented and include a quantitative comparison to NOAA-recorded tide gauge data. Second, a synoptic analysis with qualitative and quantitative evaluations of recorded data and analytical solutions is presented. The following results, analysis, and discussion was centered on the *NGOM3* simulated evolution of winds, waves, water levels, and currents for Hurricanes Ivan, Dennis, Katrina, and Isaac.

3.1. Astronomic Tides

To validate the *NGOM3* model with respect to astronomic tides across the NGOM, tidal amplitudes and phases from 43 NOAA-operated tidal stations spanning from the Florida Panhandle to Mississippi were compared to results from the *NGOM3* model. A comparison between the NOAA measured and *NGOM3* computed amplitudes and phases for the 4 dominant constituents (M2, K1, O1, Q1), separated by state, are presented in Figure 2. The NOAA measured data do include uncertainties due to coastal morphology, meteorological events, river discharge, and seasonal radiational heating patterns and can account for 35%-60% of the simulated to recorded amplitudes and 50–80% of the phase difference [*Bunya et al*., 2010]. Nonetheless, the measured to modeled amplitudes and phases for the four dominant constituents showed good agreement (Figure 2); the correlation coefficient (R^2) was 0.954 and 0.984 for the amplitude and phase, respectively (Table 2). Along the Florida Panhandle coast, the diurnal K1 and O1 constituent amplitudes were larger than semidiurnal M2 amplitudes, with the exception of Apalachicola (NOAA 8728690). The M2 constituent was equally as strong as the O1 and K1 with magnitudes greater than 0.1 m. Historically. in the eastern GoM south of Apalachicola, semidiurnal tidal propagation generally slows and tidal patterns change to diurnal dominance [*Gouillon et al*., 2010].

Along the Alabama and Mississippi coast, O1 and K1 constituent amplitudes made up the majority of the tidal amplitudes and were similar in magnitude, ~0.15–0.20 m. In Alabama, the simulated to observed amplitudes and phase showed good agreement with an R^2 of 0.977 for the amplitude and 0.984 for the phases (Table 2). Along the Mississippi coast, the largest measured to model errors were the M2 constituent phases. With respect to the observed phase, the model generally lagged the propagation of the M2 tide by ~40°; however, M2 amplitudes were small with magnitudes near 0.05 m, which make ~5% of the overall tidal amplitude along the Mississippi coast. For semidiurnal tides (*i.e*. M2), especially in a diurnal dominated region, it is difficult to extract the exact timing of the crest of the constituent's waveform when the constituent's amplitude is less than 0.05 m. Additionally, many of the tidal gauges along the Mississippi coast are located in back bays and inlets, or protected by the barrier islands and located in the shallow Mississippi Sound, and errors attributed to the simulated M2 amplitude and phase lag may have been caused by nontidal processes such as river inflow and semidiurnal daily wind- and wave-driven events that altered circulation patterns in this region. For the Mississippi measured to modeled errors, the R^2 was 0.935 and 0.977 for amplitudes and phases, respectively (Table 2).

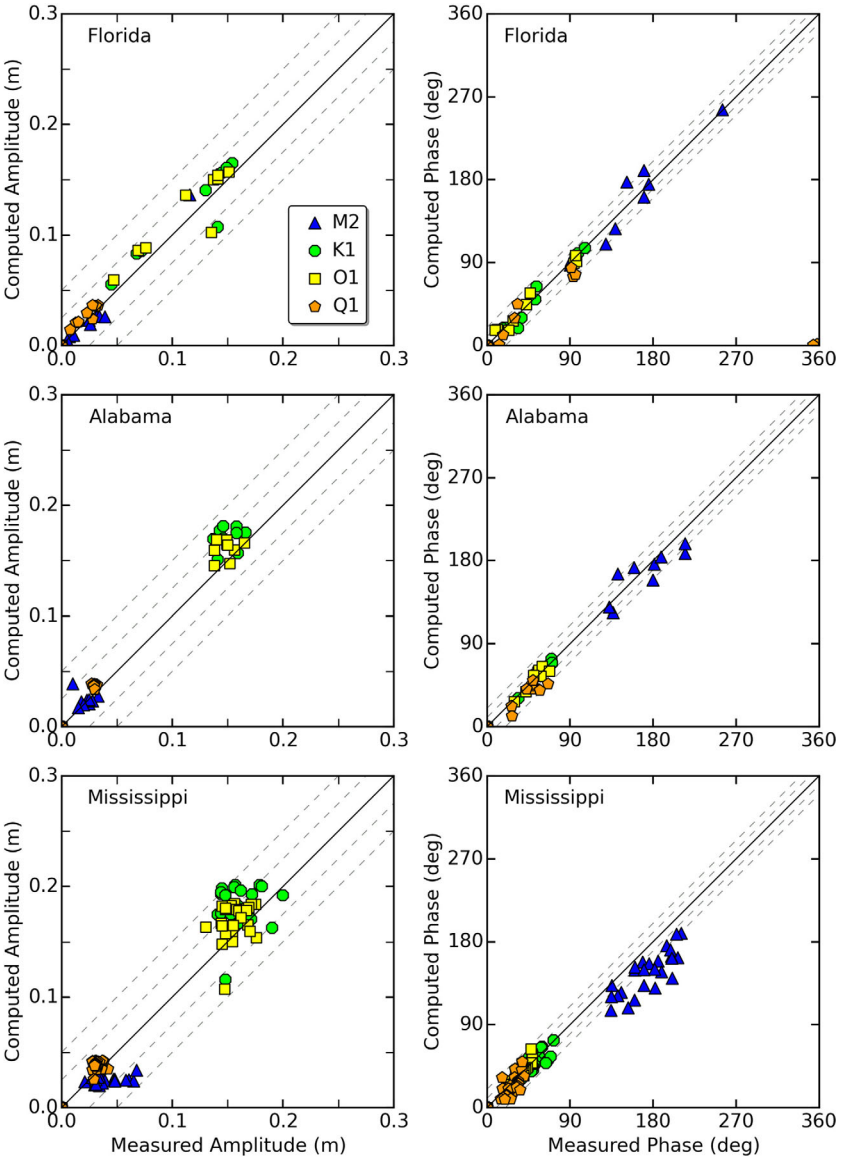

Figure 2. Comparison between *NGOM3* simulated (left) amplitudes and (right) phases to NOAA-measured astronomic tides. The results are separated by state. The error bands are 2.5 and 5 cm for the amplitudes and 10° and 20° for the phases.

Supporting information File S1 presents the tidal resynthesis results for the first spring-neap cycle of a tidal epoch (∼14.7 days) at all 43 tide gauges along the Florida Panhandle, Alabama, and Mississippi coast. Table 2 presents the *MSE/VAR* and *RMSE* among the stations separated by state. The statistics for all three states showed good agreement to the data, with the largest error for *MSE/VAR* of 0.122 in Florida, 0.058 in Alabama and 0.085 in Mississippi. The *RMSE* also indicated good agreement. The 25 stations in Mississippi resulted in an *RMSE* of 5.530 cm and Florida and Alabama had RMSE values of 4.698 cm and 4.377 cm, respectively. The errors

Table 2. Correlation Coefficient (R^2) for Amplitude and Phase, MSE/VAR, and the Root Mean Square Error (cm) Between the *NGOM3* Simulated and NOAA Observed Tides Separated by State[a]

Location	No. of Stations	R^2 Amplitude	R^2 Phase	MSE/VAR	RMSE (cm)
Florida	9	0.954	0.984	0.122	4.698
Alabama	9	0.977	0.984	0.058	4.377
Mississippi	25	0.935	0.977	0.085	5.530

[a]See supporting information File S1 for locations and 14 day tide resynthesis of the measured and modeled data.

reported were in good agreement with other tidal studies located along the east coast of the U.S. and the GoM [*Bacopoulos et al*., 2011; *Bunya et al*., 2010; *Gouillon et al*., 2010], and indicated that the daily tidal circulation processes were well resolved in the *NGOM3* model.

3.2. Hurricane Ivan (2004)

Hurricane Ivan began as a large tropical wave that moved off the West African coast on 31 August 2004 and developed into a Tropical Storm on 3 September. Ivan underwent a series of rapid intensification and weakening phases and eventually made landfall as a Category 3 (SSHS) storm at approximately 06:50 UTC 16 September, west of Gulf Shores, AL [*Stewart*, 2004]. Recorded data alongside the *NGOM3* simulated synoptic history of Hurricane Ivan are described below to understand the geophysical response in the NGOM. All values refer to the *NGOM3* simulation of Hurricane Ivan unless stated otherwise. To supplement this section, the reader is referred to supporting information Animation S1 for a comprehensive synoptic view of the winds, waves, water levels, and currents.

According to NDBC records, Hurricane Ivan generated some of the largest wave heights on record in the NGOM. Data logging at NDBC buoy 42040 (depth of 260 m) (Figure 1a) failed as the eye passed; however, the maximum value measured before failure was 15.96 m (supporting information File S2), and at the time was the largest wave height recorded by any NDBC buoy [*Wang et al*., 2005]. In deep water, prior to propagating onto the continental shelf, simulated significant wave heights were in excess of 18 m in the northeast quadrant of the storm. As the storm approached the narrow and shallow shelf, 18 m waves still persisted in the northeast quadrant of the storm, tracking northeast along the shelf break, and dissipated because of the shallow bathymetry and increase in bottom friction. Large wave heights of ~10 m persisted for over 6 h south of Santa Rosa Island near the narrow shelf. To the east of the track, buoy 42039 (depth of 300 m) recorded 12 m wave heights as the storm passed, and at a depth of 50 m, buoy 42036 recorded peak wave heights near 6.5 m (supporting information File S2); wave heights decreased with increasing distance from the storm center. In addition to increasing wave heights as the storm moved past the buoys, mean and peak wave periods also increased, and the change in wind direction induced sharp directional changes in the waves. The *NGOM3* model computed wave heights, period and direction showed good agreement to the NDBC buoys measurements (supporting information File S2).

The complicated geometry and bottom topography of the shallow WFS, Mississippi-Alabama (MSAL) shelf and the Louisiana Birds Foot generated a complex situation of currents and water levels. Figure 4 presents four snapshots in time of Hurricane Ivan's wind field and simulated de-tided water surface elevations and depth-integrated currents at 07:00 UTC 15 September (approximately 12 h before landfall) (Figures 4a and 4b), 19:00 UTC 15 September 2004 (approximately 6 h before landfall) (Figures 4c and 4d), 07:00 UTC 16 September 2004 (approximately landfall) (Figures 4e and 4f), and 13:00 UTC September 16 2004 (approximately 6 h after landfall) (Figures 4g and 4h). Figure 5a presents the time-series of wind speed and direction and Figure 5b the simulated de-tided depth-integrated currents at the seven locations (along the 25 m bathymetric contour) as shown in Figure 4.

When Ivan was located in the deep GoM (07:00 UTC 15 September 2004) winds were generally southeasterly along the west Florida coast and westerly along the northern Gulf coast (Figure 4a). Reflected by the Gulf scale winds, 1 m/s - 2 m/s depth-averaged currents were oriented counter-clockwise (CCW) in the alongshore direction across the WFS and MSAL shelf (Figure 4b). The alongshore winds across the WFS developed a minor coastally trapped wave (CTW) that propagated as a Kelvin wave north (in 25 m depth) at 8.5 m/s from Naples to Clearwater, as computed from the lag between the maximum storm surge and distance between the stations, and increased 17.0 m/s from Clearwater to Cedar Key [A detailed description of the Kelvin identification can be found in Section 3.3]. This propagation, and its speed, can also be observed from Figure 5b at Naples, Clearwater, and Cedar Key. As Ivan tracked north on 19:00 UTC 15 September 2004, storm surge of ~1.5 m had already reached the *Big Bend* region of Florida as a result of the CTW. Winds remained consistent along the west Florida coast, but near Pensacola they shifted clockwise nearly 90° to a southeasterly wind. At Horn Island and Birds Foot, the northerly wind was consistent in direction but increased in magnitude to ~20 m/s and ~35 m/s, respectively. Southerly currents of ~0.5 m/s were also consistent and were observed through ADCP observations by *Teague et al*. [2007] (Figure 5). While Ivan approached the coast and made landfall near the Alabama-Florida border, the local wind speeds near Pensacola rotated to a southerly direction and increased to over 40 m/s. The winds and currents were in

opposing directions. The wind weakened the southwesterly current but did not alter its direction (Figures 4 and 5). The momentum provided by the strong alongshore current outlasted the contribution of the local hurricane-force southerly wind.

On the left side of the storm track, the wind speeds reached their maximum several hours prior to landfall at Horn Island and Birds Foot. The northerly winds continued and, a strong outflow current of ~6 m/s was generated along the narrow and shallow shelf near the Birds Foot and was uninterrupted for ~10 h (Figure 5). This phenomenon was documented through ADCP observations by *Mitchell et al*. [2005]. Using cross-correlation, currents lagged the winds by 1.5 h and 3.0 h at Horn Island and Birds Foot, respectively, indicating currents were generally strong and aligned to the winds prior to the increase in wind speed before landfall. The southerly current near Birds Foot was caused by a combination of the existing southerly current, the large pressure gradient from the ~2.5 m storm surge along the eastern Mississippi River and within Mississippi Sound, and the increase in northerly winds prior and during landfall. From this analysis it is suggested that the large-scale winds dominate the large-scale and local circulation; however, local water surface elevation setup can influence regional circulation through water level induced pressure gradient flows. The storm created a geostrophic current that was directed CCW in the alongshore direction with the highest magnitudes on the shelf. The current was balanced by the Coriolis force and the along-shelf currents and water surface elevation gradients (pressure gradient). Even as the local wind direction rapidly changed during landfall, the local currents were unaffected for several hours after landfall as was observed near Pensacola (Figure 5).

Simulated time-series of water surface elevations are compared to observations collected from NOAA, USACE, and USGS gauge stations along the NGOM during Hurricane Ivan. Supporting information File S3 shows the locations and hydrographs for all stations and a subselection and presented in Figure 7 and their locations in Figure 3. *NGOM3* simulated water levels mimicked the rate of the rise in the surge hydrograph. Matching the rate of inundation, including the peak value and timing of the peak, indicates that topographic and bathymetric elevations in the model were correct and that bottom friction was well represented [*Dietrich et al*., 2011b]. The recession limb of the surge hydrograph was also well captured, relating back to the accurate topographic elevations and friction.

Table 3 presents a summary of the SI and relative bias for the *NGOM3* simulated time-series water levels compared to recorded data. The SI and bias at the NOAA stations were 0.281 and 0.007, and were 0.306 and 0.018 at the USACE stations, respectively. Comparing recorded and simulated peak surges at the stations yielded an R^2 of 0.58 and best-fit slope of 0.92.

A spatial comparison between field-measured HWMs and gauge peaks to the simulated maximum high water (Figure 6) is shown in Figure 8. A scatterplot comparison for the same locations is shown in Figure 9. The *NGOM3* model results were within 0.5 m at 60% of the HWMs. The slope of the line of best fit was 0.87, the R^2 was 0.53 (Table 3). The model under-predicted maximum water levels by approximately 0.5 m (or ~12% of the peak) in a cluster near Pensacola Bay (Figure 8). During Ivan, this region experienced significant barrier island overwash and overtopping [*Claudino-Sales et al*., 2010; *Kraft and de Moustier*, 2010]. Removing the stations around Pensacola Bay and Santa Rosa Sound resulted in a slope of 0.92 and R^2 of 0.81. Additionally, it cannot be certain that field measured HWMs were free from wave-driven effects (such as wave runup) because of the intense wave environment during the storm in this region. However, the model under-prediction in Pensacola Bay and Santa Rosa Sound warrants further examination, which will help us to better understand the geophysical response to Hurricane Ivan.

Hurricane Ivan caused severe morphological changes to the Alabama and Florida Panhandle coast, specifically the 85 km long Santa Rosa Island, located along the Northwestern Florida coast [*Claudino-Sales et al*., 2010]. The barrier island experienced severe overwash, defined as water and sediment across the crest of a beach or dune that does not flow back to its originating body [*Donnelly et al*., 2004], and widespread breaching. Many of the dunes, which were generally less than 4.0 m above mean sea level (MSL) prestorm, were eroded down to MSL. Poststorm field surveys discovered that much of Santa Rosa Island was completely inundated [*Claudino-Sales et al*., 2010; *Stone et al*., 2005]. During overwash, water can flow at velocities greater than 2 m/s landward, which leads to erosion of the foreshore dunes and sediment deposition landward [*Holland et al*., 1991]. When the storm tide elevation exceeds the vertical elevation of the coastal dune, the barrier becomes subaqueous and surf zone processes dominate, which are complex processes and still not well understood [*Donnelly et al*., 2004; *McCall et al*., 2010; *Sallenger*, 2000].

The *NGOM3* model was not intended and is not currently capable of describing such morphological processes. As a result, the model did not capture the breaching caused by storm-induced dune erosion. [Note, the model does include barrier island overtopping if the storm tide is greater than the elevation of the dune height.] Therefore, the model limits flow into Pensacola Bay causing under-prediction of the maximum storm tide on the backside of Santa Rosa Island and within Pensacola Bay and Santa Rosa Sound.

Fortunately, the US Geological Survey (USGS) conducted a post-Ivan lidar flight campaign along the Florida and Alabama coastal regions (http://coastal.er.usgs.gov/). The *NGOM3* mesh was modified to include elevations from the post-Ivan bare earth lidar and is referred to as the *NGOM3PI* mesh. The *NGOM3PI* mesh was placed in the same simulation setup as the original *NGOM3* Hurricane Ivan simulation, and the results of HWM and gauge peak comparison improved, 76% of the HWMs were within 0.5 m (improved from 60%). The slope of the line of best fit improved from 0.87 to 0.92 and the R^2 from 0.53 to 0.71, respectively (Table 3). Considering peak surge measurement errors (using the methods presented in *Bunya et al*. [2010]), the average absolute error and standard deviation was 0.208 m (∼5% of the peak surge) and 0.186 m for all HWMs and gauge peaks. A third simulation was performed by increasing the *NGOM3* mesh resolution by half (*i.e*. splitting each element by four) along Santa Rosa Island and including post-Ivan lidar elevations. This experiment, named *NGOM3PIx4*, was conducted to determine if the model results and respective overtopping of the barrier island were sensitive to mesh resolution. Results did not change between the *NGOM3PI* and *NGOM3PIx4* models. Moreover, simulation results may improve from additional model modifications such as surface roughness parameters that better represent post-Ivan conditions, among others; however, the *NGOM3* model was designed to incorporate the most recent data sources and to accurately simulate storm surge for a variety of events without the need for model adjustments or calibration for individual events. Because of the long time-span between Hurricane Ivan and present day, in addition to the many morphological changes that occurred from recent hurricanes, we expected that among the storms studied herein that this event would be the most challenging to model.

3.3. Hurricane Dennis (2005)

Hurricane Dennis (2005) originated off the west coast of Africa from a tropical wave on 29 June 2005. The wave achieved tropical storm strength on 5 July and became a hurricane two days later. Dennis entered the GoM on 09:00 UTC 9 July 2005 and intensified while tracking along the WFS, almost parallel to the 300 m bathymetric contour. In this section, recorded hydrodynamic data are presented alongside the *NGOM3* simulation to understand the hurricane-induced geophysical response in the NGOM. All values refer to the *NGOM3* simulation of Hurricane Dennis unless stated otherwise. To supplement this section, the reader is referred to supporting information Animation S2 for a comprehensive synoptic view of the evolution of the winds, waves, water levels, and currents.

As Dennis passed to the west of the Florida Keys, tropical storm force winds of 15 m/s - 20 m/s were directed alongshore near the Everglades, south of Marco Island and hurricane force winds were present in the northeast quadrant of the storm. Simulated significant wave heights of 8 m were generated along the WFS and grew to 11 m as the storm turned northwest and off the broad shelf into deeper water. Computed wave heights in the Big Bend region were 3 m – 6 m as wind speeds were tropical storm strength in the area. Hours before landfall, wave heights over 10 m were generated south of Pensacola and Panama City and dissipated to near 6 m waves along the narrow shelf. Dennis slightly weakened as it approached the coast and made landfall as a Category 3 storm (SSHS) on Santa Rosa Island, Florida (between Navarre Beach and Gulf Breeze) around 19:30 UTC 10 July 2005 with maximum sustained winds of 54 m/s [*Beven*, 2005]. The simulated evolution of Dennis-induced waves were validated by comparing significant wave height, mean wave period, peak wave period, and wave direction at two NDBC buoys (42003 and 42039) (Figure 1a) that recorded data during Dennis (supporting information File S4); unfortunately, all other gauges in the eastern GoM did not record wave data during Hurricane Dennis. At NDBC42003, the model matched the shape of the rise in significant wave height and captured the double peak that occurred as the storm passed the buoy. At NDBC42039 the model results agreed with the recorded data, and in particular, the evolution of significant wave height to a maximum of 11 m and mean wave period increased with increasing wave height (supporting information File S4).

The path and characteristics of Hurricane Dennis and the storms orientation with respect to the WFS excited an interesting hurricane-driven hydrodynamic response. Figure 10 presents four snapshots in time of Hurricane Dennis' wind field and simulated de-tided water surface elevation and depth-integrated currents at 01:00 UTC 10 July 2005 (approximately 18 h prior to landfall) (Figures 10a and 10b), 13:00 UTC 10 July 2005

(approximately 6 h prior to landfall) (Figures 10c and 10d), 19:00 UTC 10 July (approximately landfall) (Figures 10e and 10f), and 07:00 UTC 11 July 2005 (approximately 12 h after landfall) (Figures 10g and 10h). Figure 11a presents the time-series of wind speed and direction and Figure 11b the simulated de-tided depth-integrated currents at the seven locations (along the 25 m bathymetric contour) as shown in Figure 10.

Dennis was located off the west Florida coast at 26.3° latitude at 01:00 UTC 10 July 2005. Southeasterly winds of 20 m/s - 30 m/s persisted for nearly 12 h off the coast of Naples and were increasing near Clearwater. The winds, oriented parallel to the WFS, continued as Dennis tracked northwest and new regions along the west Florida coast became exposed to amplified southerly southeasterly winds. They continued for ∼30 hr, from 18:00 UTC 9 July 2005 to 00:00 UTC11 July 2005 (Figure 11a). Within this time frame, near 01:00 10 July 2005, a sea level anomaly of ∼1 m developed off the coast of Naples, FL (Figure 10b) along with a strong northerly alongshore current of ∼2 m/s (Figure 10b). The sea level anomaly continued north, as observed by NOAA gauge 8726724 (Clearwater Beach) (Figure 13) and propagated as a CTW along the west coast of Florida. The wave reached the Big Bend region of Florida as early as 09:00 UTC 10 July 2005 (10 h prior to landfall) and by 13:00 UTC 10 July 2005 the region experienced ∼1.75 m of storm surge (Figures 10c and 10d). The continued alongshore southeasterly winds of 20 m/s – 30 m/s amplified the anomaly [*Morey et al*., 2006], and when united with the local storm surge and high tide, generated a maximum storm tide of 2 m – 3 m in the Big Bend region (Figure 12), as recorded by station 572 and NDBC SHPF1 (Shell Point) (Figure 13). This storm tide was ∼1 m higher than that generated at landfall near Pensacola (Figure 10e).

As was found with Hurricane Ivan (section 3.2), Hurricane Dennis generated strong alongshore currents with the largest magnitudes along the shelf. Even as the local wind direction rapidly changed during landfall, current directions were generally unaffected. This was observed at Apalachicola, Pensacola, Horn Island, and Birds Foot; however, the currents were reduced after landfall due to the opposing direction of the local wind and current (Figure 11). Additionally, a 2 m/s – 3 m/s outflow current was simulated near the Birds Foot and, although reduced in magnitude to ∼0.75 m/s 12 h after landfall and a change in wind direction, it continued in a southerly direction (Figures 10h and 11). The large-scale wind fields of Hurricane Dennis produced a geostrophic current with a balance between the Coriolis force and the along-shelf currents and pressure gradient (water surface elevation gradient). It was this balance that generated the CTW across the WFS.

We further investigate the CTW using the *NGOM3* model solution. First, the Ekman setup along the west Florida coast was estimated from the Coriolis frequency, f, (0.66×10^{-4} s^{-1} at 27° latitude), the depth-averaged along-shelf velocity, V, and the shelf distance, x [*Freeman et al*., 1957; *Kennedy et al*., 2011]:

$$\eta_c = \int {}^{fV}/_{g} dx \tag{6}$$

Using a shelf distance of 200 km and the average depth-averaged cross-shelf velocity from the *NGOM3* model solution, the resulting Ekman setup, η_c, was 0.86 m. The large setup at the coast was caused from northerly longshore currents of ∼0.75 m/s that persisted across the WFS (Figures 10 and 11). At 04:30 UTC 10 July 2005, the setup along the coast was 0.89 m as computed by the *NGOM3* model and agrees with the estimate of 0.86 m using equation (6). Plotting the de-tided *NGOM3* simulated water surface elevation in the cross-shelf direction at 2 h intervals beginning at 02:30 UTC 10 July to 08:30 UTC 10 July shows the classic exponential decay of water level with increasing across-shelf distance from the coast (Figure 14). This is a result of the geostrophic balance of the longshore velocity and water surface elevation gradient. The distance where the wave amplitude is substantial is within an e-folding distance of the coast and is on the order of the Rossby Deformation Radius, R_d:

$$R_d = \frac{c}{f} = {}^{\sqrt{gh}}/_{f} \tag{7}$$

where c is wave speed and h is the average depth across the shelf [*Pedlosky*, 1992; *Wang*, 2003]. Taking h as 15 m and computing the shallow water wave speed, the Rossby Deformation Radius is ∼180 km at 27° latitude, which is of similar scale to the WFS width (200 km) [*Mitchum and Sturges*, 1982]. The e-folding length scale of ∼180 km can also be observed from the cross-shelf water surface elevation profile shown in Figure 14. This indicates that the shallow WFS contributed to the generation of the sea level anomaly. The coastline provided a boundary for the wave to "lean" on as it propagated north as coastally trapped Kelvin waves rely upon a shallow shelf whereas other Kelvin waves only depend upon a coast [*Pedlosky*, 1992].

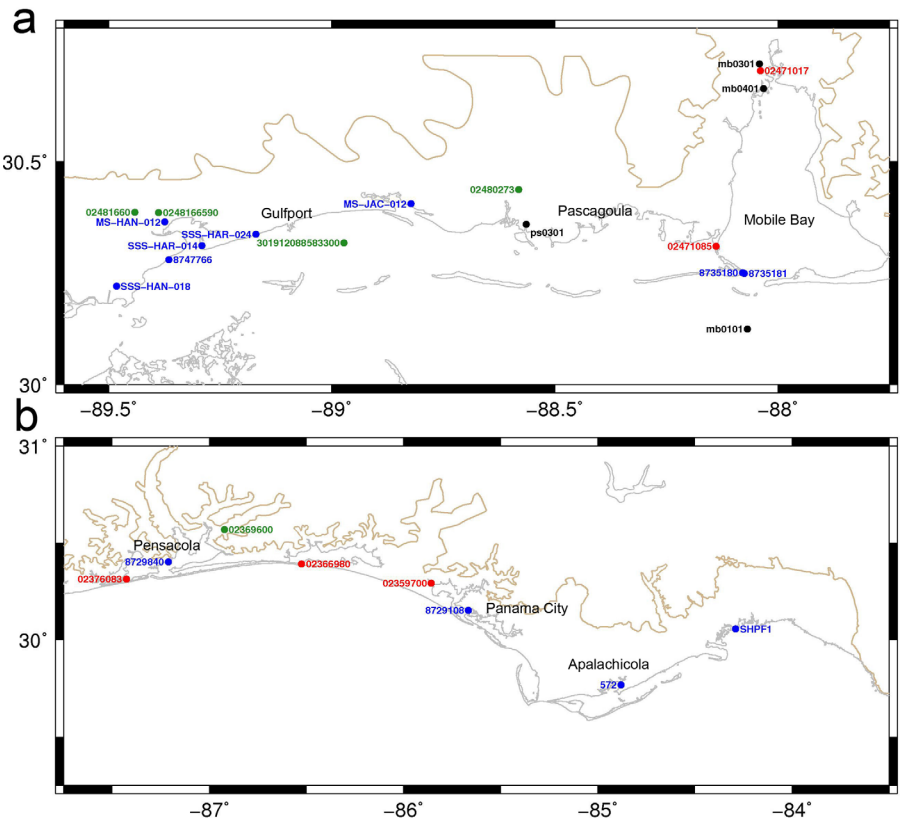

Figure 3. Locations of NOAA and rapid storm tide sensors (SSS) (blue), USACE (red), USGS (green), and depth-integrated current gauges (black) for which hydrographs and statistics are shown in Table 3 along (a) Mississippi and Alabama and (b) the Florida Panhandle.

We also compared the shallow water wave speed of the along coast propagating wave to the phase speed by computing the cross-correlation of the de-tided *NGOM3* simulated water levels along the west Florida coast. The phase speed was computed between Naples (NOAA 8725110), Clearwater (NOAA 8726724) and Cedar Key (NOAA 8727520), and was determined from the lag time and distance between stations. Lag time was computed from the maximum cross-correlation of the de-tided storm surge hydrograph. Between Naples and Clearwater the computed lag time was 7.25 h with a phase speed of 8.8 m/s and from Clearwater to Cedar Key the lag time was 4.0 h with phase speed was 8.58 m/s. This propagation speed is on the order the shallow water wave speed (12 m/s in 15 m depth) and yields an e-folding length scale of ∼130 km (Figure 12), on the order of the Rossby radius using the shallow water wave speed (180 km). Interestingly, the phase speed was nearly equivalent to the forward speed of Hurricane Dennis (8.2 m/s). The estimated first-mode wave speed applied to the WFS is 8.2 m/s and is at its maximum amplification when the storm's forward speed is equal to the phase speed [*Clarke*, 1977; *Clarke and Van Gorder*, 1986; *Mitchum and Clarke*, 1986; *Morey et al*., 2006], which aligns with the *NGOM3* model solution.

Furthermore, *NGOM3* simulated time-series water levels compared to measured data at NOAA gauges 8726724, 8727520), and NDBC SHPF1 (Figure 13) demonstrated that the model accurately captures the propagation of the wave along the WFS and the wave interaction and peak surge within Apalachee Bay. To assess model accuracy with the NGOM region, simulated water levels were compared to additional NOAA, NDBC, and USGS stations (Figure 3) that recorded time series water levels during Hurricane Dennis (supporting information File S5). The model results matched well with the observed values and matched the evolution of the surge in time and in magnitude, and the SI and bias were 0.259 and −0.072, respectively (Table 3). The small forerunner was captured at NOAA8726724 and NOAA8727520 along the west coast of Florida in addition to the surge drawdown at station NOAA8729840, and the peak surges at station 572, NDBC SHPF1, and NOAA 8729108 (Figure 13 and supporting information File S5). Among the time-series water levels, the average absolute difference and standard deviation were 0.126 m (0.088 m including measurement error) and 0.186 m (0.123 m including measurement error), respectively (Table 3).

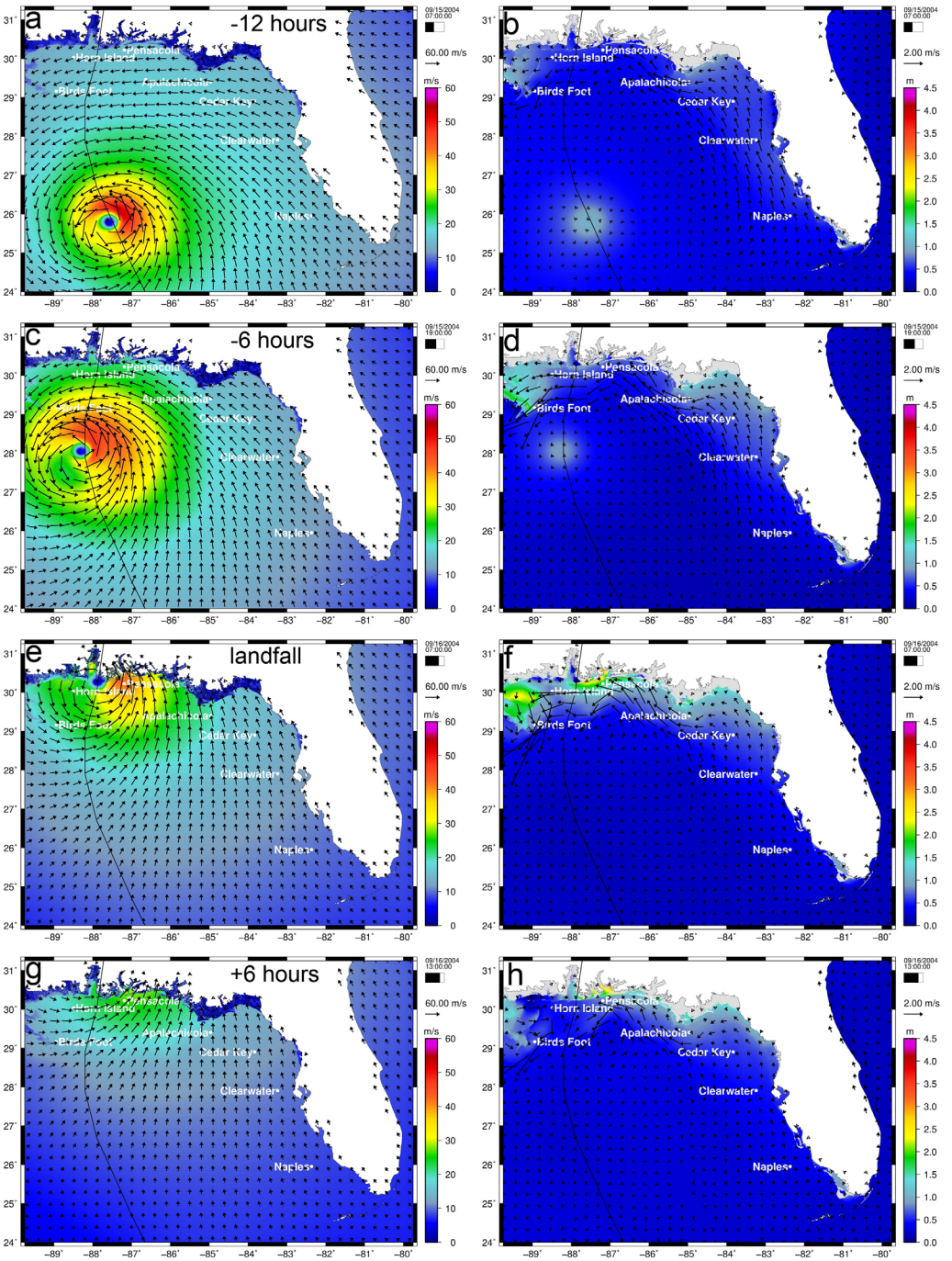

Figure 4. (a, c, d, e) Wind speeds (m/s) and de-tided simulated water surface elevation contours (m, NAVD88) and (b, d, f, h) depth-averaged current vectors (m/s) during Hurricane Ivan at (a, b) 07:00 UTC 15 September 2004, approximately 12 h before landfall; (c, d) 19:00 UTC 15 September 2004, approximately 12 h before landfall; (e, f) 07:00 UTC 16 September, approximately at landfall; and (g, h) 13:00 UTC 16 September 2004, approximately 6 h after landfall.

The region surrounding Apalachicola and Apalachee, FL experienced the largest water levels on the order of 2 m – 3 m (Figure 12); near landfall, maximum water levels were on the order of 1–2 m. In addition to time-series water levels, simulated maximum water levels were compared to poststorm FEMA collected measured HWMs and gauge peak surge (Figure 8). As previously described, HWMs containing errors or wave effects were removed along with measured errors outside of the IQR (section 3.2). Out of the 142 HWMs, modeled maximum surge were within 0.25 m at 55% and 99% are within 0.5 m of the measured

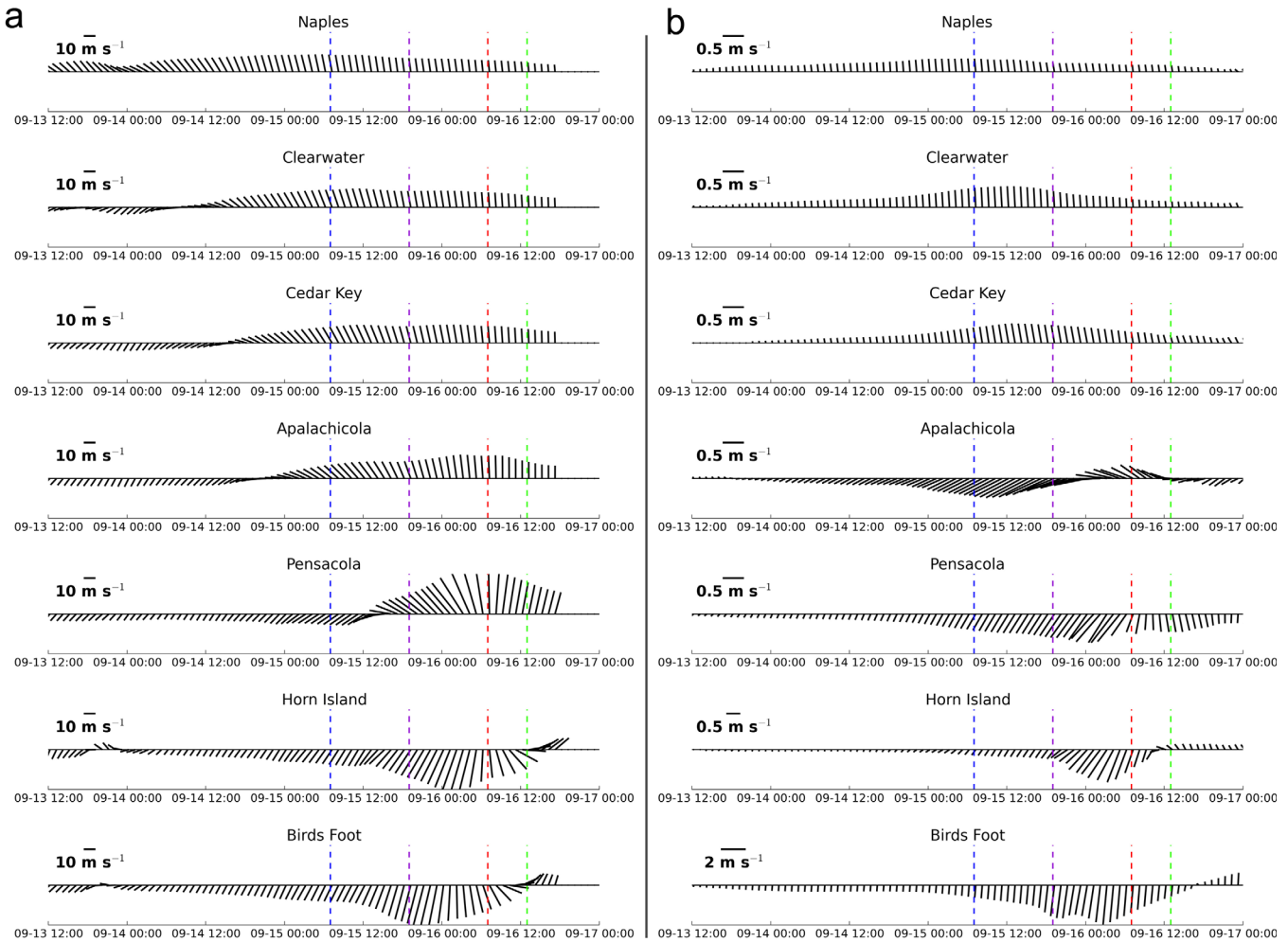

Figure 5. (a) Wind speeds and direction and (b) de-tided simulated current speeds and directions for the seven locations located along the 25 m bathymetric contour as shown in (Figure 4). The vectors are at hourly intervals from 12:00 UTC 13 September to 9 September 2004 and oriented such as north is the top of the page. The horizontal lines represent the snapshots as shown in Figure 5. The blue line is on 07:00 UTC 15 September 2004, approximately 24 h before landfall; purple is 19:00 UTC 15 September 2004, approximately 12 h before landfall; red is 07:00 UTC 16 September, approximately at landfall; and green is 13:00 UTC 16 September 2004, approximately 6 h after landfall.

value. A scatter plot comparison is shown in Figure 9. The line of best fit had a slope of 0.93, the R^2 was 0.73 (Table 3). The average absolute error was 0.231 m and a standard deviation of 0.246 m. For all stations and HWMs and accounting for measurement error, the average absolute difference was 0.151 m and the standard deviation is 0.115 m.

3.4. Hurricane Katrina (2005)

Numerous studies have been published that simulate Hurricane Katrina-driven waves and water levels with focus on southern Louisiana and Mississippi, but not along the Alabama and Florida coast [*Bunya et al.*, 2010; *Dietrich et al.*, 2011a; *Ebersole et al.*, 2010; *Kim et al.*, 2008]. Regions of coastal Alabama and within Mobile Bay experienced 3 m - 4.5 m of storm surge and portions of the Florida Panhandle witnessed 0.6 m – 1.8 m of surge [*Knabb et al.*, 2005]. In many areas, the surge from Katrina was larger than Hurricanes Ivan and Dennis along the Alabama and Florida Panhandle coast, yet they still remain largely unstudied.

Hurricane Katrina (2005) was one of the most devastating (deadliest and costliest) natural disasters in U.S. history. Katrina originated from a complex interaction of a tropical wave, remnants of Tropical Depression 10, and an upper tropospheric trough. The system developed into a tropical depression across the Bahamas on 23 August 2005 and became a hurricane at 21:00 UTC 25 August 2005. As Katrina entered the GoM, the storm continued to strengthen and reached Category 5 status (SSHS) by 12:00 UTC 28 August 2005 with

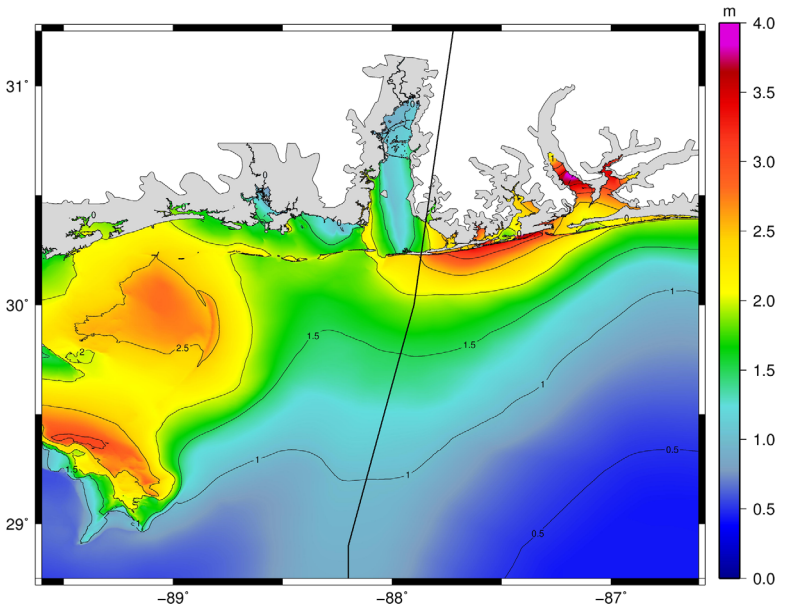

Figure 6. Hurricane Ivan *NGOM3* simulated maximum water levels (m) along the Mississippi, Alabama, and western Florida Panhandle.

winds near 78 m/s. Katrina was a large storm with hurricane force winds extending out to 167 km and tropical storm force winds 370 m from the center. Katrina made its second landfall as a strong Category 3 (SSHS) storm near Buras, LA at 11:00 UTC 29 August and made its third and final landfall near the Louisiana-Mississippi border with estimated winds of 54 m/s [*Knabb et al.*, 2005]. Recorded data alongside the *NGOM3* simulated synoptic history of Hurricane Katrina are described below to understand the geophysical response in the NGOM. All values refer to the *NGOM3* simulation of Hurricane Katrina unless stated otherwise. To supplement this section, the reader is referred to supporting information Animation S3 for a comprehensive view of the evolution of the winds, waves, water levels, and currents.

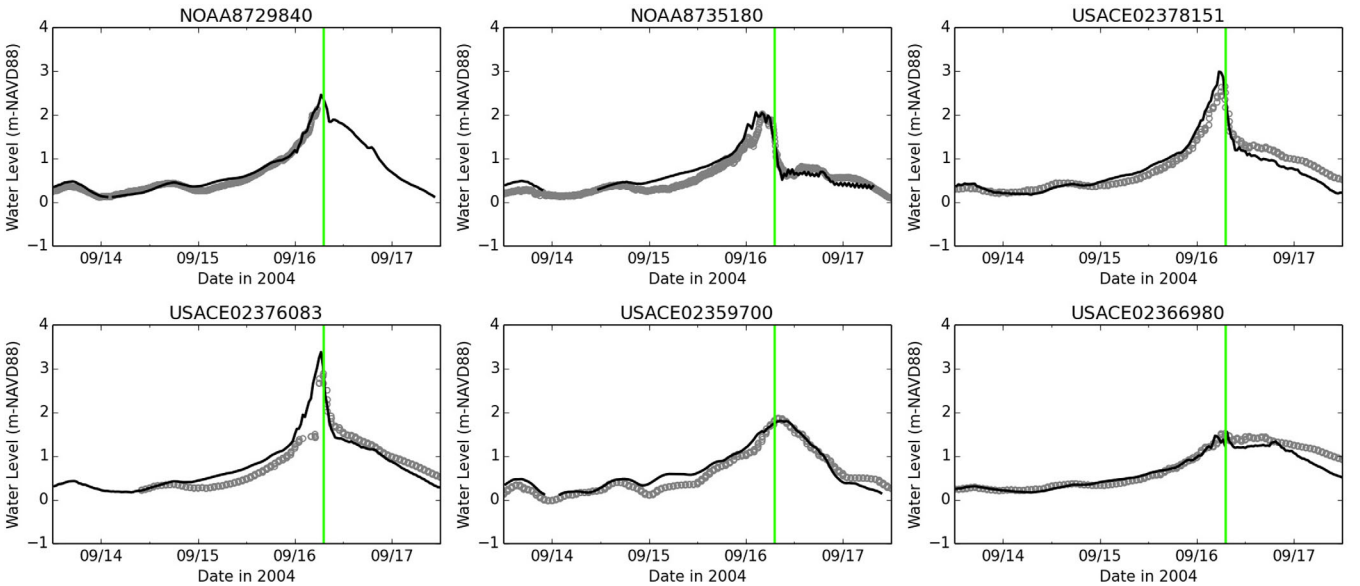

Figure 7. *NGOM3* modeled (black line) and gauge measured (gray circles) water surface elevation time series during Hurricane Ivan for a select number of stations. See supporting information File S3 for hydrographs at all stations. Landfall is represented by the green vertical line.

Table 3. Summary of *NGOM3* Water Level Statistics for All Recorded Water Level Measurements for All Storms[a]

					ADCIRC to Measured HWMs					Measured HWMs		Estimated ADCIRC Errors	
Storm	Data Source	No. of Stations	SI	Bias	No. of HWMs	Slope	R^2	Avg. Abs. Diff.	Std. Dev.	Avg. Abs. Diff.	Std. Dev.	Avg. Abs. Diff.	Std. Dev.
Ivan	NOAA	6	0.281	0.070									
	USACE	17	0.306	0.018	11	0.92	0.58	0.311	0.372				
	FEMA				126	0.87	0.50	0.449	0.497	0.137	0.229	0.312	0.268
	All	23	0.299	0.031	137	0.87	0.53	0.438	0.490	0.144	0.227	0.295	0.263
Ivan (NGOM3PI)	NOAA	6	0.283	0.073									
	USACE	17	0.303	0.019	11	0.91	0.58	0.318	0.380				
	FEMA				126	0.92	0.70	0.347	0.403	0.116	0.199	0.232	0.204
	All	23	0.298	0.033	137	0.92	0.71	0.345	0.401	0.137	0.215	0.208	0.186
Dennis	NOAA/NDBC	14	0.248	−0.071	14	0.96	1.02	0.096	0.105	0.048	0.068	0.048	0.037
	FEMA				142	0.93	0.73	0.231	0.246	0.043	0.076	0.188	0.170
	All				156	0.93	0.77	0.219	0.242	0.068	0.126	0.151	0.115
Katrina	NOAA	9	0.238	−0.002									
	USACE	16	0.200	0.011	12	0.94	0.95	0.117	0.139	0.070	0.074	0.047	0.065
	USGS	7	0.206	−0.065									
	FEMA				312	1.00	0.96	0.269	0.344	0.178	0.201	0.090	0.143
	All	32	0.212	−0.009	324	1.00	0.97	0.263	0.336	0.174	0.196	0.089	0.140
Isaac	NOAA	16	0.256	0.043	16	1.02	0.95	0.079	0.088	0.001	0.002	0.078	0.086
	USGS Perm.	14	0.264	−0.105	13	1.06	0.85	0.204	0.193				
	USGS SSS	45	0.195	−0.051	39	1.05	0.92	0.157	0.133	0.030	0.048	0.128	0.084
	USGS Rapid	6	0.226	−0.027									
	NOAA HWM				42	0.94	0.73	0.256	0.284	0.068	0.132	0.187	0.152
	All	81	0.221	−0.040	110	0.99	0.85	0.189	0.242	0.053	0.095	0.136	0.147

[a]SI and bias were only computed for time-series data. Average absolute difference and standard deviation are in meters. Statistics and errors for peak storm surge were only computed if the data set had 10 reliable stations.

Hurricane Katrina generated some of the largest significant wave heights ever recorded by NDBC buoys; NDBC buoy 42040 measured a wave height of 16.91 m (supporting information File S6), surpassing the record previously held by Ivan at 15.96 m. Other NDBC buoys in the eastern Gulf also recorded large wave heights of near 11 m at buoy 42003, before capsizing, and ~8 m at buoy 42001 and 42039 (supporting information File S6). In line with the increase in wave height, the peak wave period increased at all buoys to

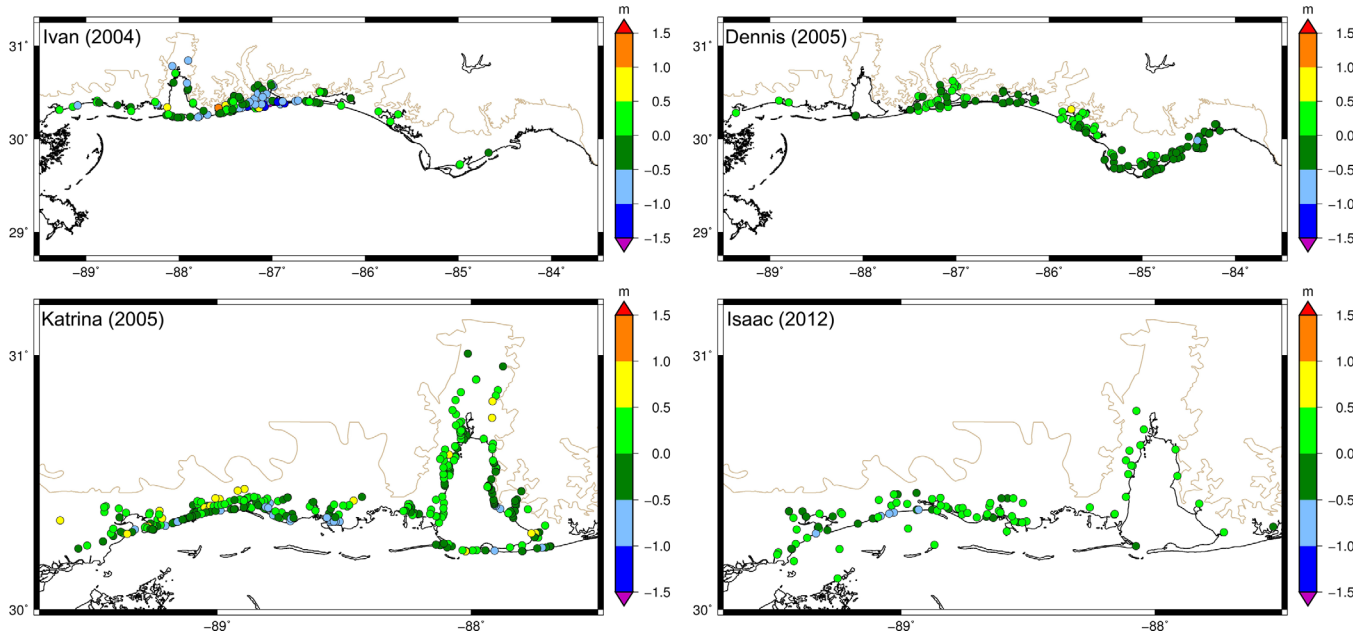

Figure 8. Spatial comparison of high water marks and gauge peaks for Hurricanes Ivan, Dennis, Katrina, and Isaac. The HWMs are colored according to maximum water surface elevation errors. Green points indicate an error of ± 0.5 m.

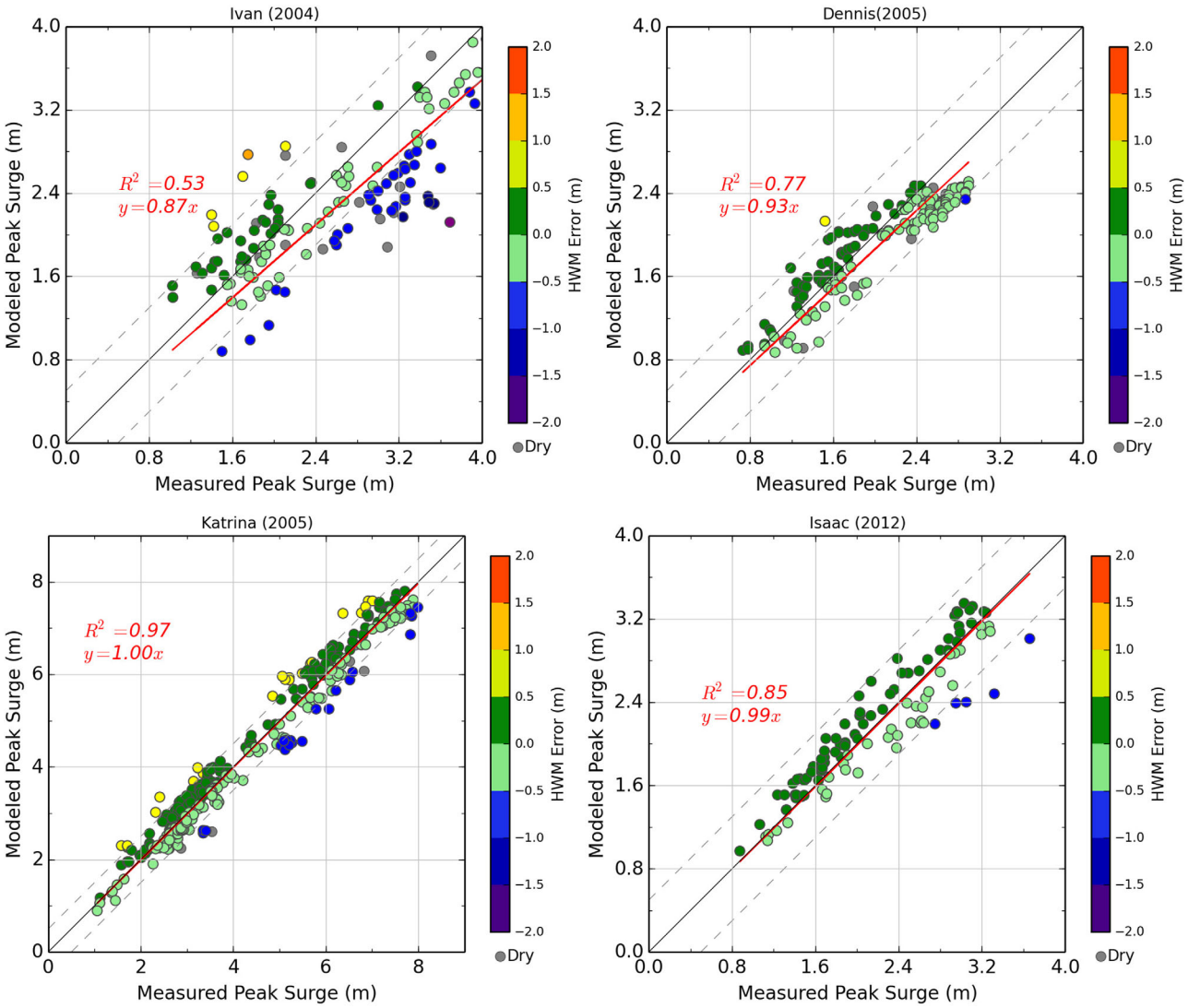

Figure 9. Scatterplot of high water marks and gauge peaks for Hurricanes Ivan, Dennis, Katrina, and Isaac. The HWMs are colored according to maximum water surface elevation errors. Green points indicate an error of ± 0.5 m.

∼15 s until the storm passed several days later (supporting information File S6). Near the coast, large wave heights up to 18 m were simulated to the south of the Bird's Foot and dissipated as they propagated across the MS-AL shelf. The Mississippi, Alabama, and Florida barrier islands diminish wave heights and limit wave propagation into the Mississippi Sound, Mobile Bay, and the various back bays (supporting information Animation S3). Simulated time-series of significant wave height, peak and average wave period, and wave direction showed good agreement to recorded data at six NDBC buoys in the eastern GoM during Hurricane Katrina (supporting information File S6).

Figure 15 presents four snapshots in time of Hurricane Katrina's wind field and simulated de-tided water surface elevation and depth-integrated currents at 09:00 UTC 28 August 2005 (approximately 30 h prior to landfall) (Figures 15a and 15b), 09:00 UTC 29 August 2005 (approximately 6 h prior to landfall) (Figures 15c and 15d), 15:00 UTC August 29 2005 (approximately landfall at the Louisiana-Mississippi border) (Figures 15e and 15f), and 21:00 UTC 29 August 2005 (approximately 6 h after landfall) (Figures 10g and 10h). Figure 16a presents the time-series of wind speed and direction and Figure 16b the simulated de-tided depth-integrated currents at the seven locations (along the 25 m bathymetric contour) as shown in Figure 15.

Prior to 09:00 UTC 28 August 2005, winds along the WFS shifted from a northerly to southerly direction as Katrina progressed into the GoM. A northerly alongshore depth-averaged current of ∼0.75 m/s was

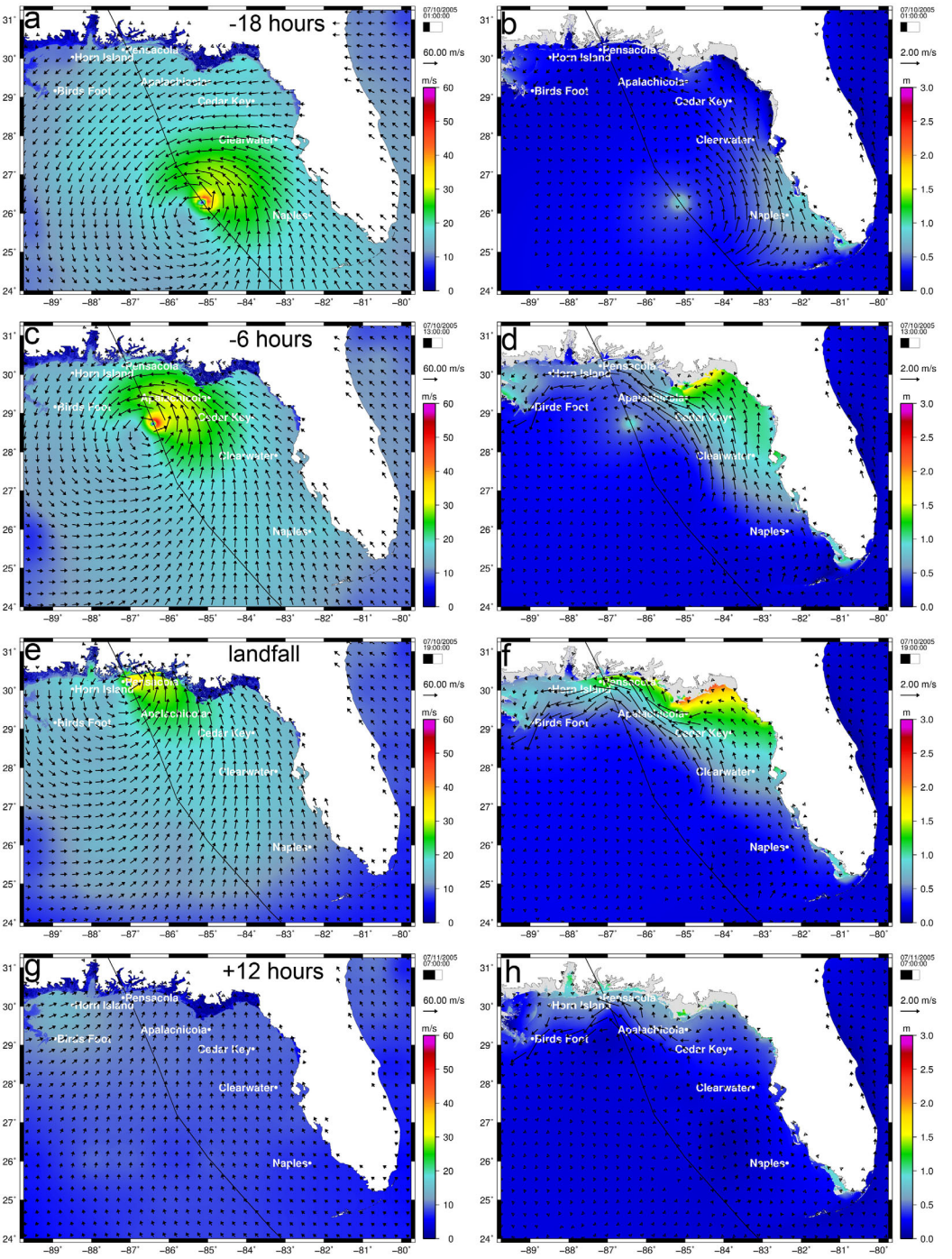

Figure 10. (a, c, d, e) Wind speeds (m/s) and de-tided simulated water surface elevation contours (m, NAVD88) and (b, d, f, h) depth-averaged current vectors (m/s) during Hurricane Dennis at (a, b) 01:00 UTC 10 July 2005, approximately 18 h before landfall; (c, d) 13:00 UTC 10 July 2005, approximately 6 h before landfall; (e, f) 19:00 UTC 20 July 2005, approximately at landfall; and (g, h) 07:00 11 July 2005, approximately 12 h after landfall.

developed along the WFS. At Naples, the change in current direction lagged the winds by ~6 hr; however, the currents at Clearwater and Cedar Key shifted prior to the winds changing direction (Figures 16a and 16b). This was caused by a minor CTW that propagated along the WFS at ~11 m/s. The CTW reached Clearwater and Cedar Key prior to the shift in the local wind direction and caused a northerly alongshore current. Northeasterly currents shifted to a southwesterly direction at Apalachicola ~5 h prior to the change in wind direction near 09:00 UTC 28 August 2005 as the CTW turned west along the Florida Panhandle and traveled

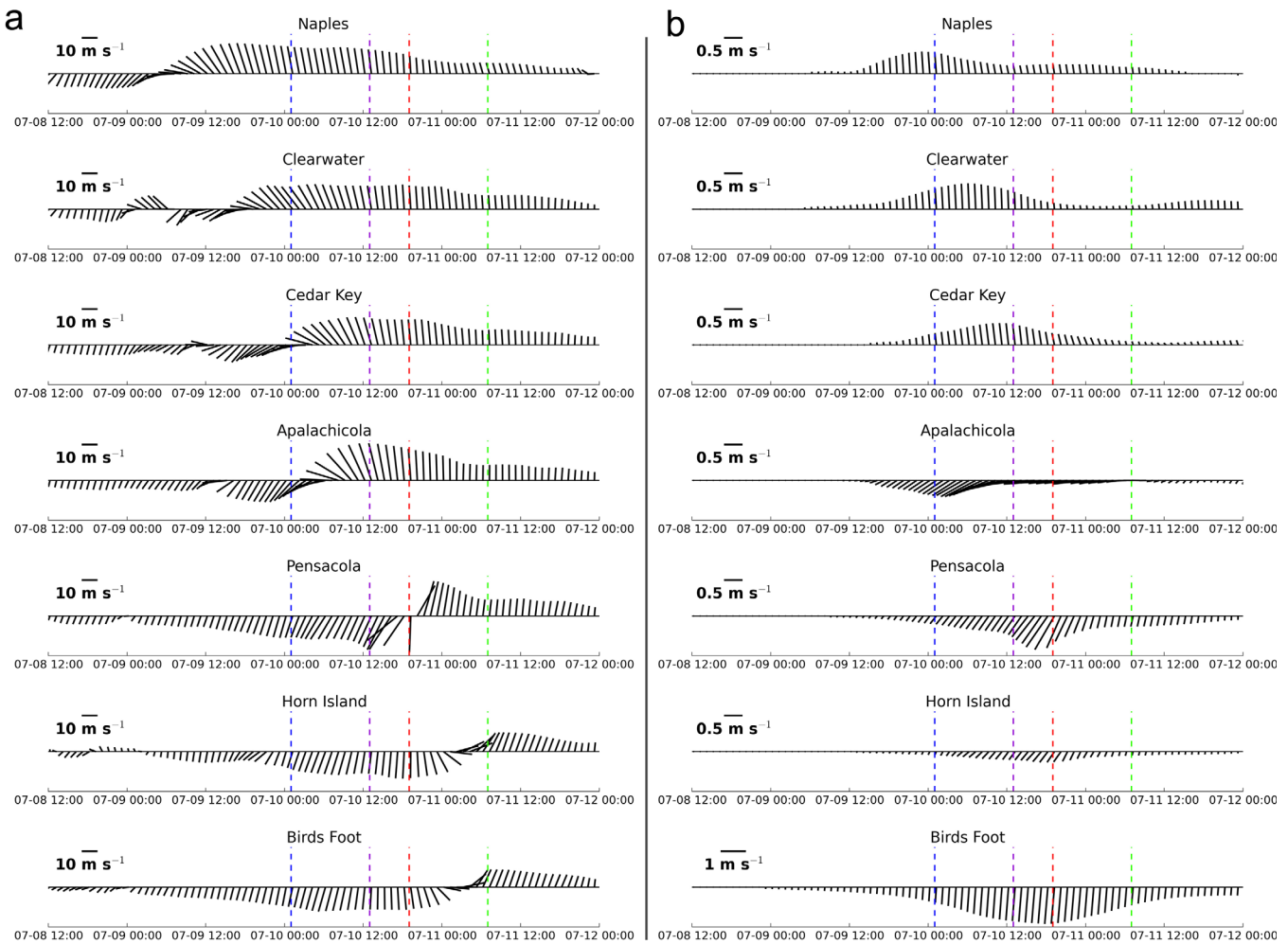

Figure 11. (a) Wind speeds and direction and (b) de-tided simulated current speeds and directions for the seven locations located along the 25 m bathymetric contour as shown in (Figure 10). The vectors are at hourly intervals from 12:00 UTC 8 July to 00:00 12 July 2005 and oriented such as north is the top of the page. The horizontal lines represent the snapshots as shown in Figure 10. The blue line is on 01:00 UTC 10 July 2005, approximately 18 h before landfall; 13:00 UTC 10 July 2005, approximately 6 h before landfall; red is 19:00 UTC 20 July 2005, approximately at landfall; and green is 07:00 11 July 2005, approximately 12 h after landfall.

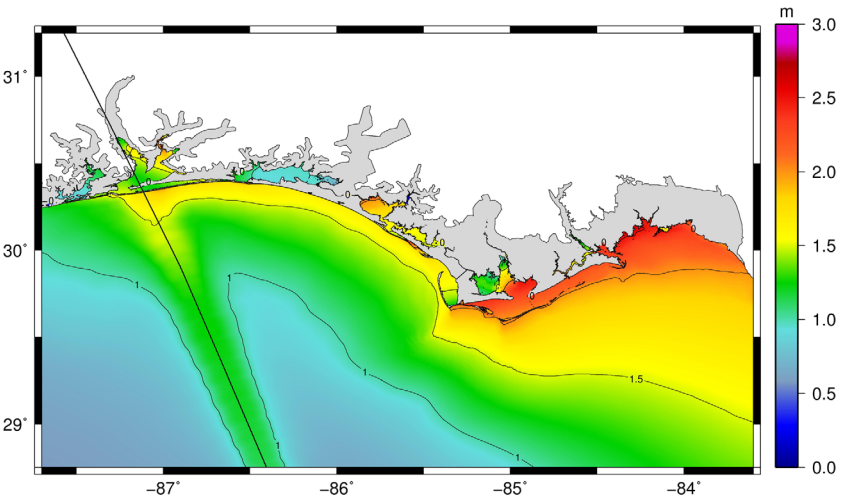

Figure 12. Hurricane Dennis *NGOM3* simulated maximum water levels (m) along the Florida Panhandle.

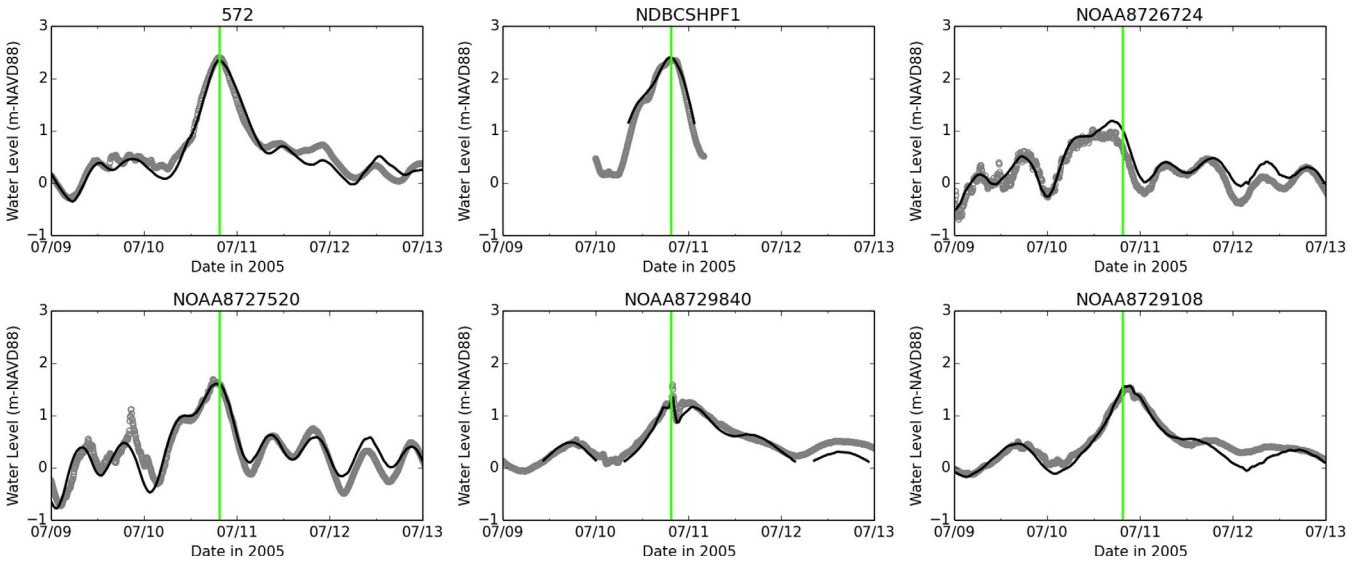

Figure 13. *NGOM3* modeled (black line) and gauge measured (gray circles) water surface elevation time series during Hurricane Dennis for a select number of stations. See supporting information File S5 for hydrographs at all stations. Landfall is represented by the green vertical line.

at a speed of 12.2 m/s, computed between Apalachicola to Pensacola via cross-correlation. As a result of the CTW, the currents at Pensacola, on 09:00 UTC 28 August 2005, increased and shifted southwesterly (along-shelf direction), nearly 9 h after the winds transferred from a northeast to southwest direction. The along-shelf currents continued to increase at Pensacola even as the southerly winds increased to over 20 m/s by 09:00 UTC 29 August 2005 (Figure 16).

By 09:00 UTC August 29, 6 h prior to landfall, the storm tide along the western Mississippi coast was already rising and was captured by NOAA gauge 8747766 (Waveland, MS) and NOAA 8743281 (Ocean Springs, MS) (Figure 17). A 3.5 m storm surge began to build within the Biloxi marsh and along the eastern Mississippi River. Winds were generally out of the southwest with magnitudes greater than 60 m/s and were accompanied by a persistent 2.0 m/s alongshore current across the shelf that was oriented CCW (Figures 15c and 15d). Also during this time, the Bay of St. Louis was rapidly swelling, and surge was being moved up the Jordan and Wolf River. Before 12:00 UTC 29 August, the easterly winds pushed surge over Mississippi Highway 43 near Shoreline Park and the storm surge rapidly increased along the Mississippi coast. At Horn Island and Birds Foot, northeasterly winds quickly increased and shifted southerly by Katrina's final landfall at 15:00 UTC 29 August 2005 along the Louisiana-Mississippi border. The strong southerly winds caused northerly depth-averaged currents with magnitudes upward of 5.0 m/s south of Mississippi (Figure 16). The combination of surge that was contained within the Biloxi marsh and against the eastern Mississippi River, the high southerly winds, and northerly currents generated a storm tide over 7 m along the Mississippi coast and continued to increase for the next 2 h (Figures 15e and 15f), peaking near 7.5 m near Pass Christian and greater than 8 m in northern Bay of St. Louis near I-10 at 16:00 UTC 29 August (Figure 18). In fact, flooding in Pass Christian converged from both the ocean and bay side and much of the area north of I-10 near Diamondhead flooded from the backside, not the bay side. The rise in storm surge occurred within

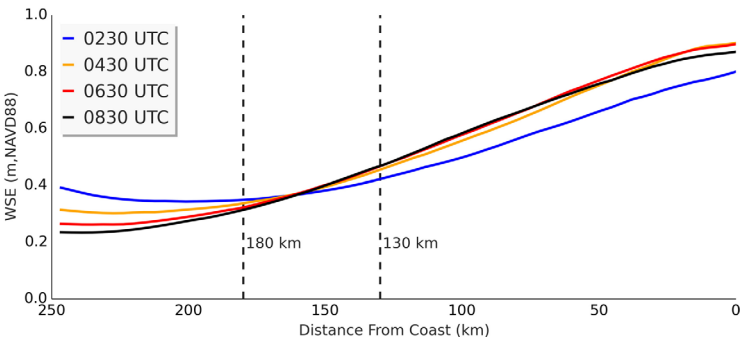

Figure 14. *NGOM3* simulated water surface elevation (m) across the WFS with increasing distance from the coast at different times on 10 July 2005. The characteristic of a coastal Kelvin wave is the exponential decay to the Rossby Radius of Deformation, which is on the order of 130 km to 180 km.

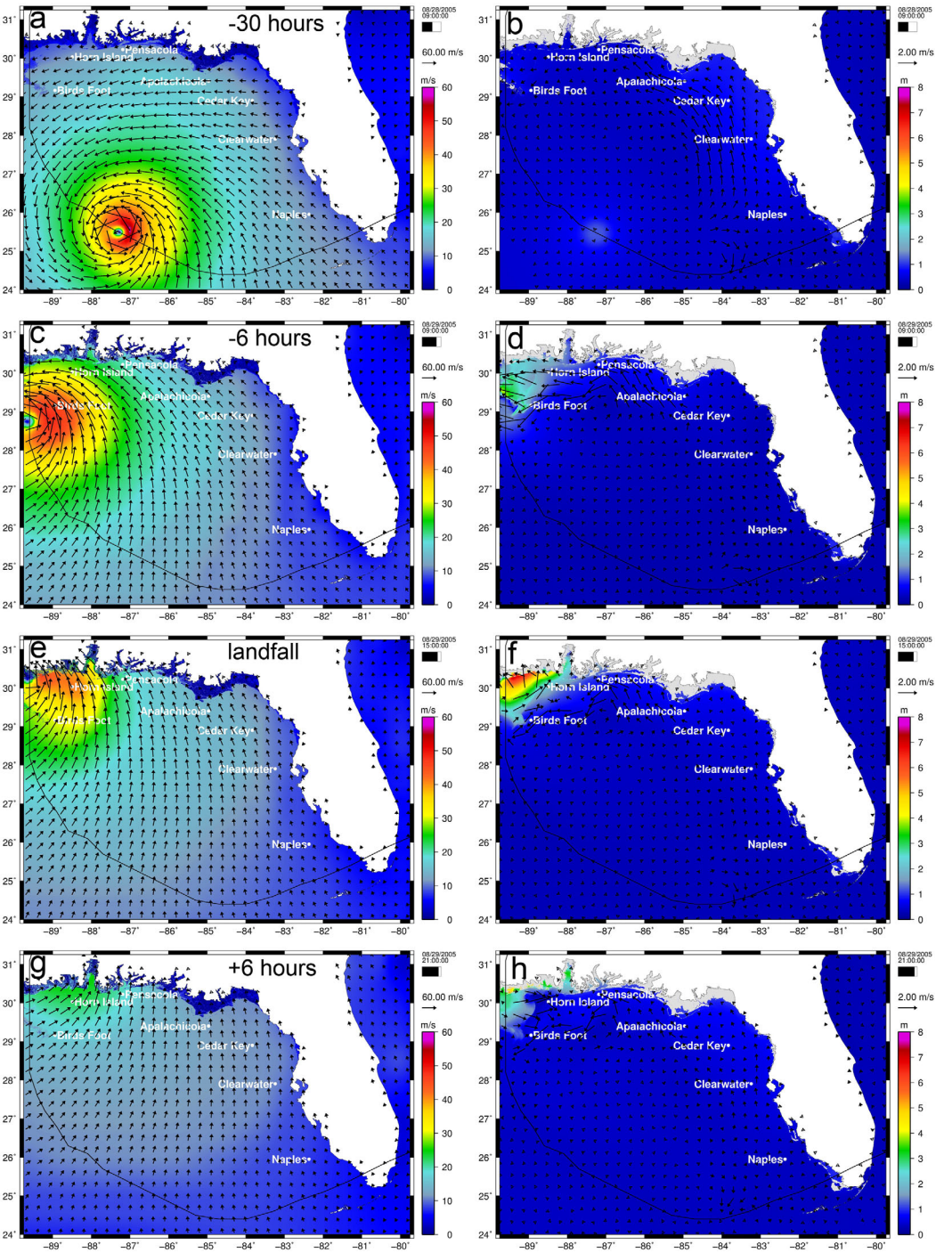

Figure 15. (a, c, d, e) Wind speeds (m/s) and(b, d, f, h) de-tided simulated water surface elevation contours (m, NAVD88) and depth-averaged current vectors (m/s) during Hurricane Katrina at (a, b) 09:00 UTC 28 August 2005, approximately 30 h before landfall; (c, d) 09:00 UTC 29 August 2005, approximately 6 h before landfall; (e, f) 15:00 UTC 29 August 2005, approximately at landfall along the Louisiana-Mississippi border; and (g, h) 21:00 29 August 2005, approximately 6 h after landfall.

a time span of nearly 6–8 h (Figures 15d and 15f). Also, while Katrina made landfall, 35 m/s southerly winds moved water up the Pascagoula River and marsh and against US90 in Pascagoula, MS. Wind directions shifted southwest and pushed the surge into Mobile Bay from within Mississippi Sound (USACE 2471017 and USACE 2471085) (Figure 17). Along the western Florida Panhandle locally generated wind setup resulted in ~2 m surge in Perdido and Pensacola Bay (NOAA 8729840) (Figure 17).

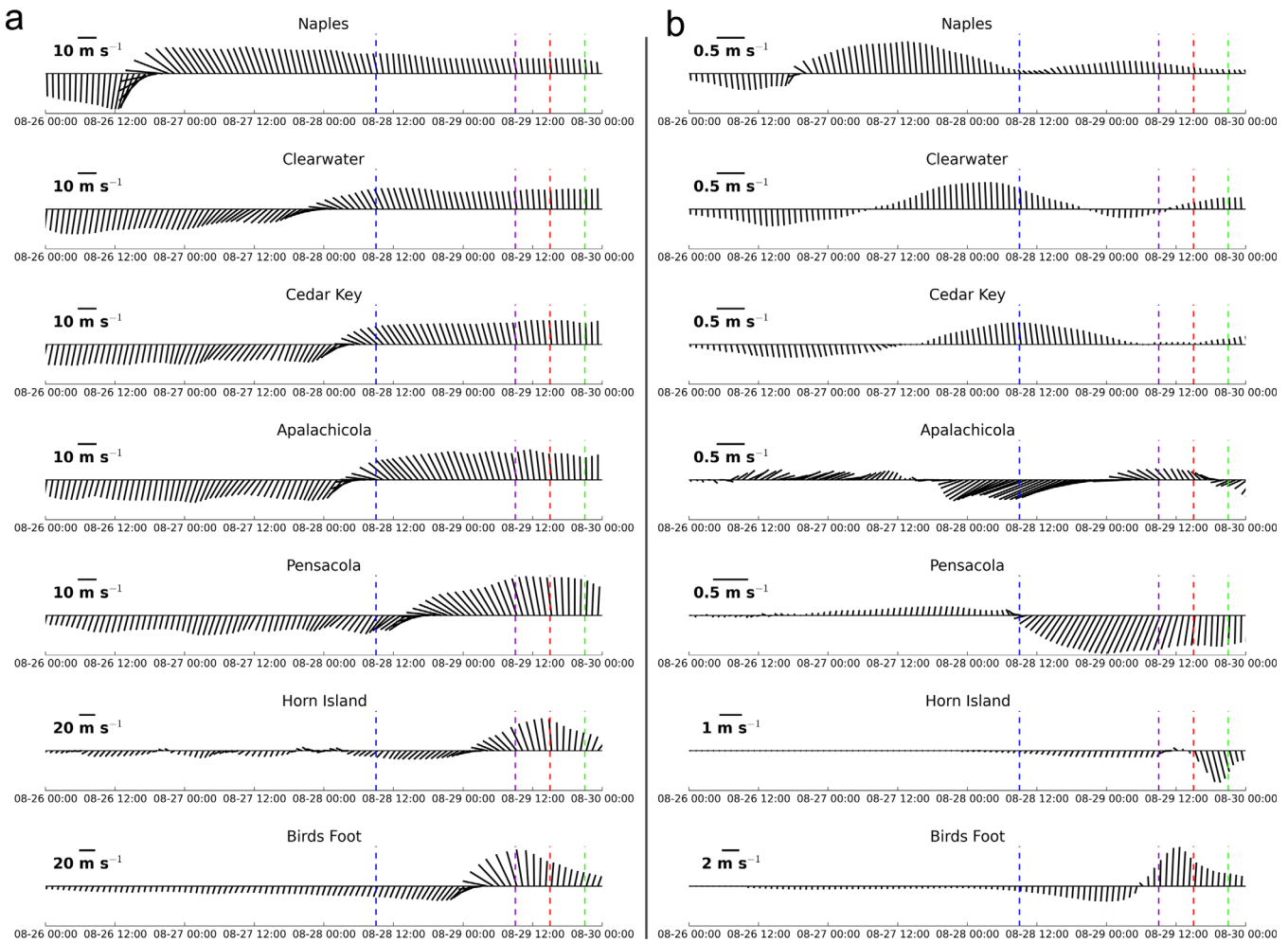

Figure 16. (a) Wind speeds and direction and (b) de-tided simulated current speeds and directions for the seven locations located along the 25 m bathymetric contour as shown in (Figure 15). The vectors are at hourly intervals from 00:00 UTC 26 August 2005 to 00:00 30 August 2005 and oriented such as north is the top of the page. The horizontal lines represent the snapshots as shown in Figure 15. The blue line is on 09:00 UTC 28 August 2005, approximately 30 h before landfall; 09:00 UTC 29 August 2005, approximately 6 h before landfall; red is 15:00 29 August 2005, approximately at landfall; and green is 21:00 29 August 2005, approximately 6 h after landfall.

Hurricane Katrina generated a multifaceted state of currents and water levels along the complex geometry of the GoM. As Katrina evolved in the Gulf, the local winds that generated the geostrophic current caused the depth-averaged currents to rotate their direction prior to the change in the local wind field (Figure 16). Therefore, it is suggested that the large-scale winds of Katrina dominated at the Gulf-scale and local circulation and induced a minor CTW along the WFS and MS-AL shelf that propagated with a speed of ~12 m/s. As found with Hurricane Ivan and Hurricane Dennis, the storm created a CCW geostrophic current across the continental shelf with a balance between the Coriolis force and the along-shelf currents and water level gradient.

NGOM3 simulated time-series water levels agreed with the measured water levels throughout the Mississippi, Alabama, and western Florida Panhandle coast (supporting information File S7). Overall, simulated water levels agreed with the measurements in the peak storm tide, and time of peak, as well as the slope of the rising and falling limb (Figure 17). This was especially important due to the large and rapid rise in water level during Katrina. Less accurate results, such as USGS 023690660 were caused by lack of mesh resolution. These stations are located in small upstream channels, and could not be sufficiently described without drastically increasing local model resolution. Other discrepancies between model and measured water levels were station datum conflicts (unknown datum) or influence of river inflow. However, the mean SI and relative bias were 0.219 and −0.002 (Table 3). Comparison of measured and modeled station peaks resulted in an R^2 of 0.89 and the slope of the line-of-best-fit was 1.06.

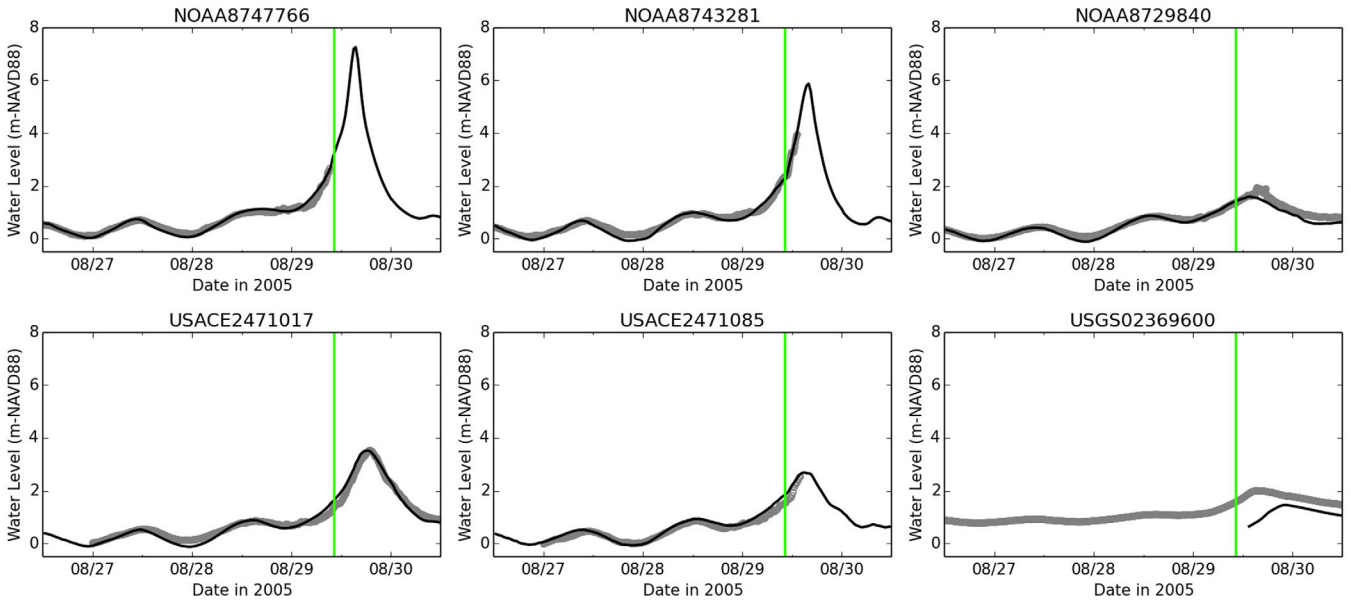

Figure 17. *NGOM3* modeled (black line) and gauge measured (gray circles) water surface elevation time series during Hurricane Katrina for a select number of stations. See supporting information File S7 for hydrographs at all stations. Landfall is represented by the green vertical line.

The high model skill was also demonstrated through a HWM analysis by comparing measured to simulated maximum water levels (Figure 8). After removing erroneous HWM measurements and HWMs with wave runup influences along the Mississippi and Alabama coast, 304 HMWs remained. The *NGOM3* model was within +/- 0.25 m at 56% of the HWMs and within +/− 0.5 m at 89% of the HWMs (Figure 8). The model resulted in a HWM average absolute difference error of 0.252 m and standard deviation of 0.317 m (Table 3). The slope of the line of best fit was 1.00 and R^2 was 0.97 among all HWMs and gauge peaks (Figure 9). When including measurement error the average absolute difference and standard deviation were 0.089 and 0.140, respectively (Table 3).

3.5. Hurricane Isaac (2012)

Hurricane Isaac (2012) began as a tropical wave off the west coast of Africa on 16 August 2012. It developed into a tropical depression at 06:00 UTC 21 August 1160 km off the west coast of the Lesser Antilles. Over the next 12 h the system strengthened into a tropical storm. Isaac gradually strengthened prior to landfall to a Category 1 (SSHS) storm near 12:00 28 UTC August. At this time, Isaac's forward speed drastically

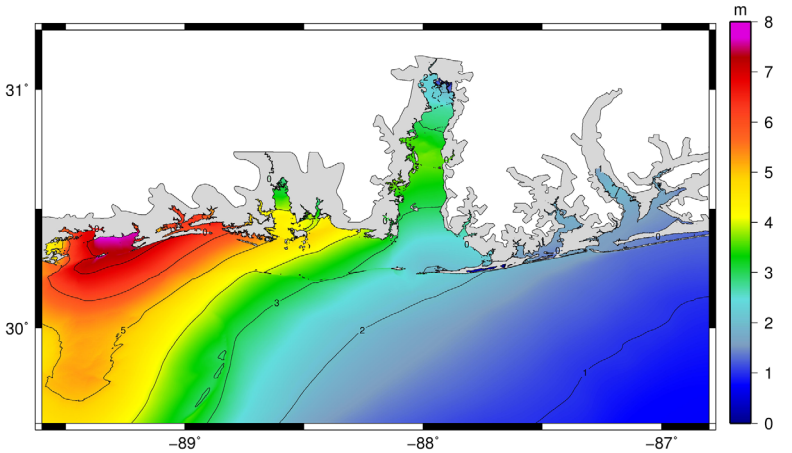

Figure 18. Hurricane Katrina *NGOM3* simulated maximum water levels (m) along the Mississippi, Alabama, and western Florida Panhandle coast.

slowed causing long periods of intense winds, storm surge, and rainfall [*Berg*, 2012]. In addition to NDBC buoys recording wave data, the USGS, in conjunction with FEMA, deployed a suite of 172 temporary water-level monitoring gauges across the Louisiana, Mississippi, and Alabama coast [*McCallum et al*., 2012] (supporting information File S9). The water level data were collected via the USGS Storm Tide Mapper (http://water.usgs.gov/floods/) and *McCallum et al*. [2012]. Recorded data alongside the *NGOM3* simulated synoptic history of Hurricane Isaac are described below to understand the geophysical response in the NGOM. All values refer to the *NGOM3* simulation of Hurricane Isaac unless stated otherwise. To supplement this section, the reader is referred to supporting information Animation S4 for a comprehensive synoptic view of the winds, waves, water levels, and currents.

Figure 19 presents four snapshots in time of Hurricane Isaac's wind field and simulated de-tided water surface elevations and depth-integrated currents at 00:00 UTC 28 August 2012 (approximately 24 h before landfall) (Figures 4a and 4b), 12:00 UTC 28 August 2005 (approximately 12 h before landfall) (Figures 4c and 4d), 00:00 UTC 29 August 2012 (approximately landfall at the Mississippi River Delta) (Figures 4e and 4f), and 12:00 UTC 29 August 2012 (approximately 12 h after landfall) (Figures 4g and 4h). Figure 20a presents the time-series of wind speed and direction and Figure 20b the simulated de-tided depth-integrated currents at the seven locations (along the 25 m bathymetric contour) as shown in Figure 19.

As Isaac tracked to the northwest aimed for the mouth of the Mississippi River, winds along the WFS shifted to a ~15 m/s southeasterly wind early on 27 August 2005. The shift in the winds, near Naples, generated a northerly alongshore current and the persistent south-southeasterly winds along the WFS and excited a CTW. The CTW reached Clearwater hours prior to 00:00 28 August 2005 and then propagated as a coastally trapped Kelvin wave to Cedar Key (Figure 20). The signature of the Kelvin wave can be observed in Figure 20b at Naples, Clearwater, and Cedar Key as well as in Figure 19b with the ~1.0 m sea level anomaly that was generated along the WFS. The maximum positive cross-correlation of the water level time-series of the stations was computed to determine the speed of the CTW. The average propagation speed was 14 m/s between Naples and Clearwater and 17 m/s between Clearwater and Cedar Key. This yields an e-folding distance of ~218 km at 28° latitude, the location of Clearwater (the Coriolis force is 0.71×10^{-4} s^{-1} at 28° latitude). The phase speed was slightly faster than that excited during Hurricane Dennis and was more than likely attributed to the slow forward speed of Isaac (~3.5 m/s), compared to Dennis (8.2 m/s), as well as the tracks more westerly direction. Additionally, inertial oscillations (defined by $2\pi/f$ and equal to 24.5 h in the GoM), caused by the abrupt arrival of the wind field [*Le*, 1994], were observed in the simulated depth-averaged currents in Figure 19b. The oscillations are clear at Naples, Clearwater, and Cedar Key.

On 12:00 UTC 29 August 2005 Isaac was 12 h away from its landfall on the Mississippi River Delta. The CTW wave generated ~1.5 m storm surge in the *Big Bend* region, similar to the Kelvin wave response during Hurricane Dennis. Easterly winds across the NGOM increased to ~20 m/s and were rapidly shifting clockwise to a southerly wind. Currents along the Florida Panhandle increased to ~2.0 m/s as well as along the Mississippi-Louisiana shelf through the Birds Foot (Figures 19b, 19c, and 20). The CTW that moved along the WFS turned to the west and propagated from Apalachicola to Pensacola with a phase speed of 6.5 m/s, which yields an e-folding distance of 85 km (the Coriolis force is 0.71×10^{-4} s^{-1} at 30° latitude). The e-folding distance is similar to the width of the continental shelf along the Florida Panhandle, which is ~90 km, half of the WFS width.

During landfall on 00:00 29 August 2005, winds were primarily southerly along the NGOM, with higher wind speeds over 30 m/s near landfall at Horn Island and Birds Foot (Figure 19e). Easterly winds and ~2.0 m/s westerly currents across the Mississippi-Louisiana shelf caused surge to accumulate in western Mississippi, within the Biloxi marsh and along the eastern Mississippi River (Figure 19f). There were also southwesterly currents over 5 m/s near Birds Foot hours prior to landfall caused by the earlier northeasterly winds, but then diminished and changed direction ~6 h after the winds moved in a southerly direction during landfall (Figure 20). As Isaac tracked northeast 12 h after landfall, over 30 m/s southeasterly winds moved the surge that was within the Biloxi marsh and against the eastern Mississippi River toward the Mississippi-Louisiana border into the Biloxi Bay and the Bay of St. Louis. *NGOM3* properly simulated the maximum storm tide across the Mississippi coast that occurred late on August 29, as observed by station SSS-MS-HAR-014 and SSS-MS-HAR-024, with water levels reaching ~3.5 m in the back of the Bay of St. Louis, as recorded by SSS-MS-HAN-012, USGS 0248166590, and USGS 02481660 (Figure 21). Even as surge began to recede in much of the region, the *NGOM3* simulated surge still continued to move upstream (north) in the Pascagoula River

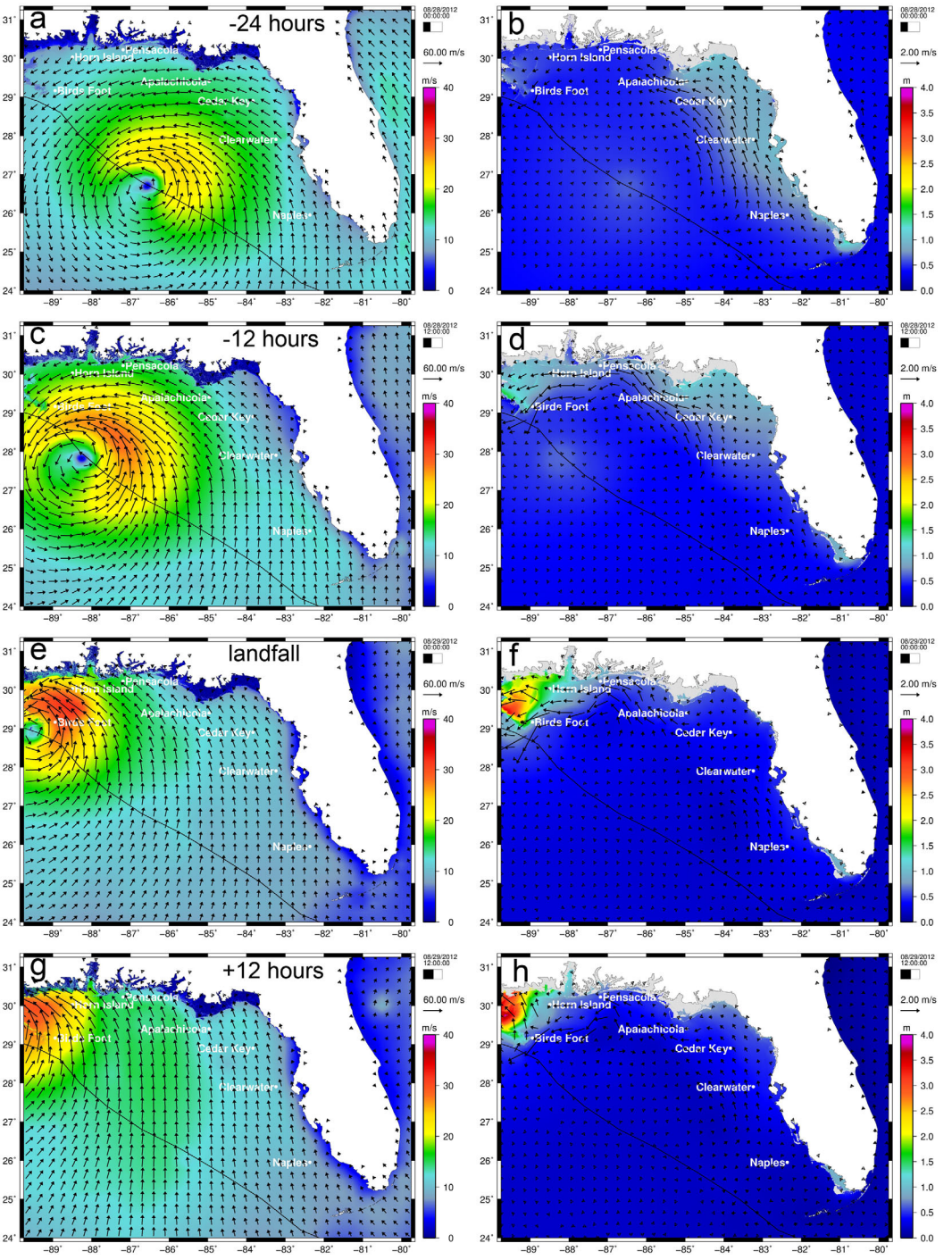

Figure 19. (a, c, d, e) Wind speeds (m/s) and(b, d, f, h) de-tided simulated water surface elevation contours (m, NAVD88) and depth-averaged current vectors (m/s) during Hurricane Isaac at (a, b) 00:00 UTC 28 August 2012, approximately 24 h before landfall; (c, d) 12:00 UTC 28 August 2012, approximately 12 h before landfall; (e, f) 00:00 UTC 29 August 2012, approximately at landfall at the Mississippi River Delta; and (g, h) 12:00 29 August 2012, approximately 12 h after landfall.

and adjacent marsh, as observed at USGS 02480273 (Figure 21). Offshore at Horn Island, currents continued to persist in the southerly direction (Figure 20b) and currents to the south (south of the Mississippi barrier island) were moving easterly (Figure 19h). Also, currents at the Birds Foot station were directed north and were aligned with the wind, south and southeast of Birds Foot the currents were stronger at over 2.0 m/s and were traveling southwest, opposite the wind direction (Figures 19g and 19h).

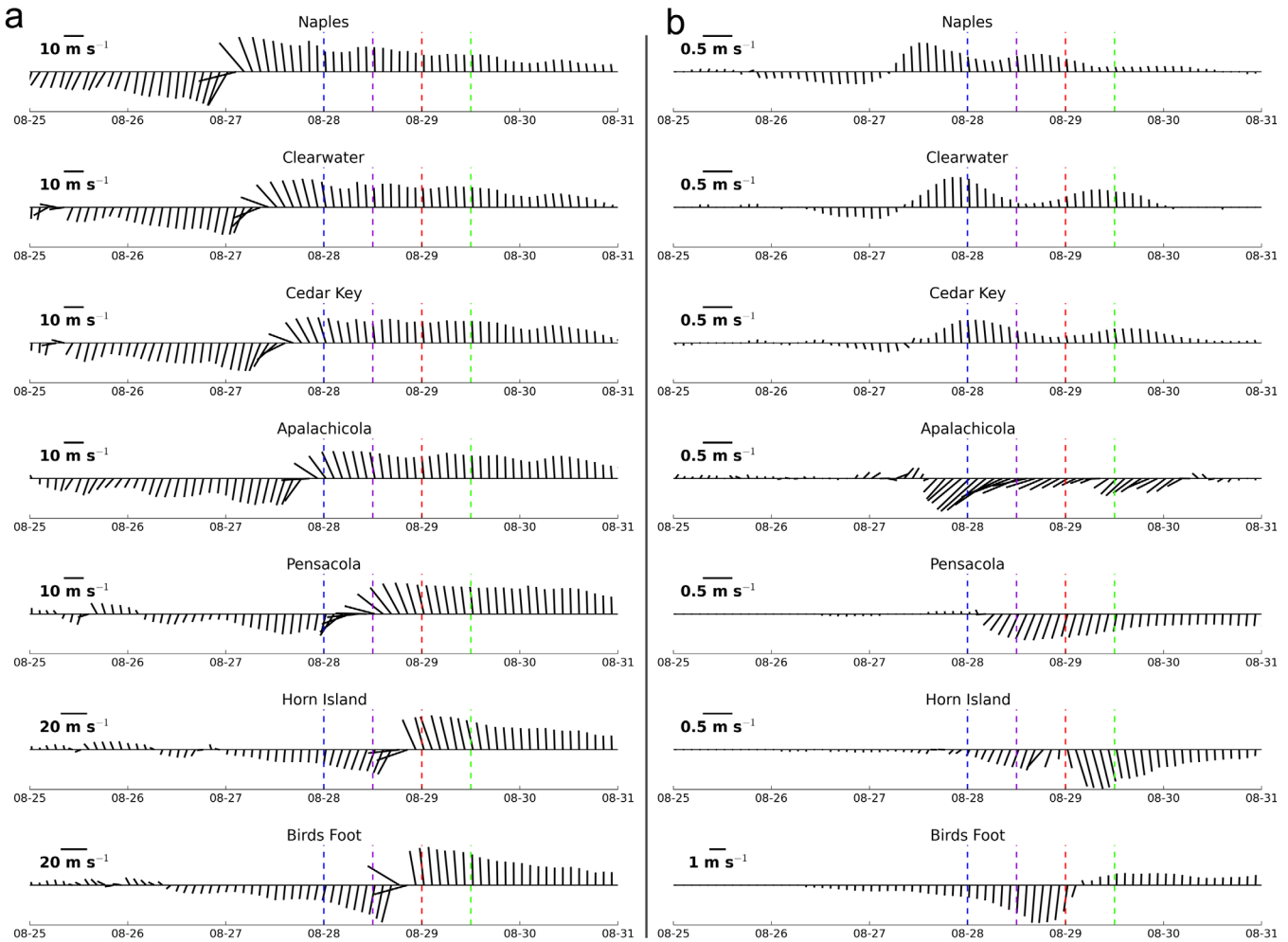

Figure 20. (a) Wind speeds and direction and (b) de-tided simulated current speeds and directions for the seven locations located along the 25 m bathymetric contour as shown in (Figure 19). The vectors are at hourly intervals from 00:00 UTC 25 August 2012 to 00:00 31 August 2005 and oriented such as north is the top of the page. The horizontal lines represent the snapshots as shown in Figure 19. The blue line is on 00:00 UTC 28 August 2012, approximately 24 h before landfall; 12:00 UTC 28 August 2012, approximately 12 h before landfall; red is 00:00 29 August 2012, approximately at landfall at the Mississippi River Delta; and green is 12:00 29 August 2012, approximately 12 h after landfall.

Similarly observed in the *NGOM3* model simulation from the previous storms, Hurricane Isaac generated a complex condition of water levels and currents. Isaac caused a CTW to propagate along the WFS as well as along the shelf south of the Florida Panhandle with e-folding distances similar to respective shelf width. The CTW was caused by a geostrophic current that balanced the Coriolis force with the currents and water level pressure gradient. The CCW orientation of the currents was driven by the large-scale wind patterns, but in areas such as south of the Mississippi barrier island and south of Birds Foot, the along-shelf currents persisted and outlasted the rapid change in wind direction during Isaac's landfall. This suggests that the large-scale hurricane-induced wind field is the dominant driver for the regional and local circulation pattern.

The recorded data at the NDBC buoys, NOAA tide stations, and USGS gauges allowed a thorough *NGOM3* model validation in Mississippi, Alabama, and Florida. In all, measured and modeled data are compared at NDBC buoys (supporting information File S8), NOAA gauges, permanent USGS gauges, rapid deployed storm tide sensors (SSS), and rapid deployment USGS streamgauges (supporting information File S9). Unfortunately, the NDBC buoys to the east of the storm track south of Mississippi failed. Nonetheless, the *NGOM3* simulated values matched well the measured wave data, especially along the WFS (NDBC 42099 and 42036) (supporting information File S8).

Overall, simulated time series water levels agreed with recorded data at the NOAA, and USGS storm tide and streamgauges. Figure 21 shows the comparison of the measured and modeled data at a select set of

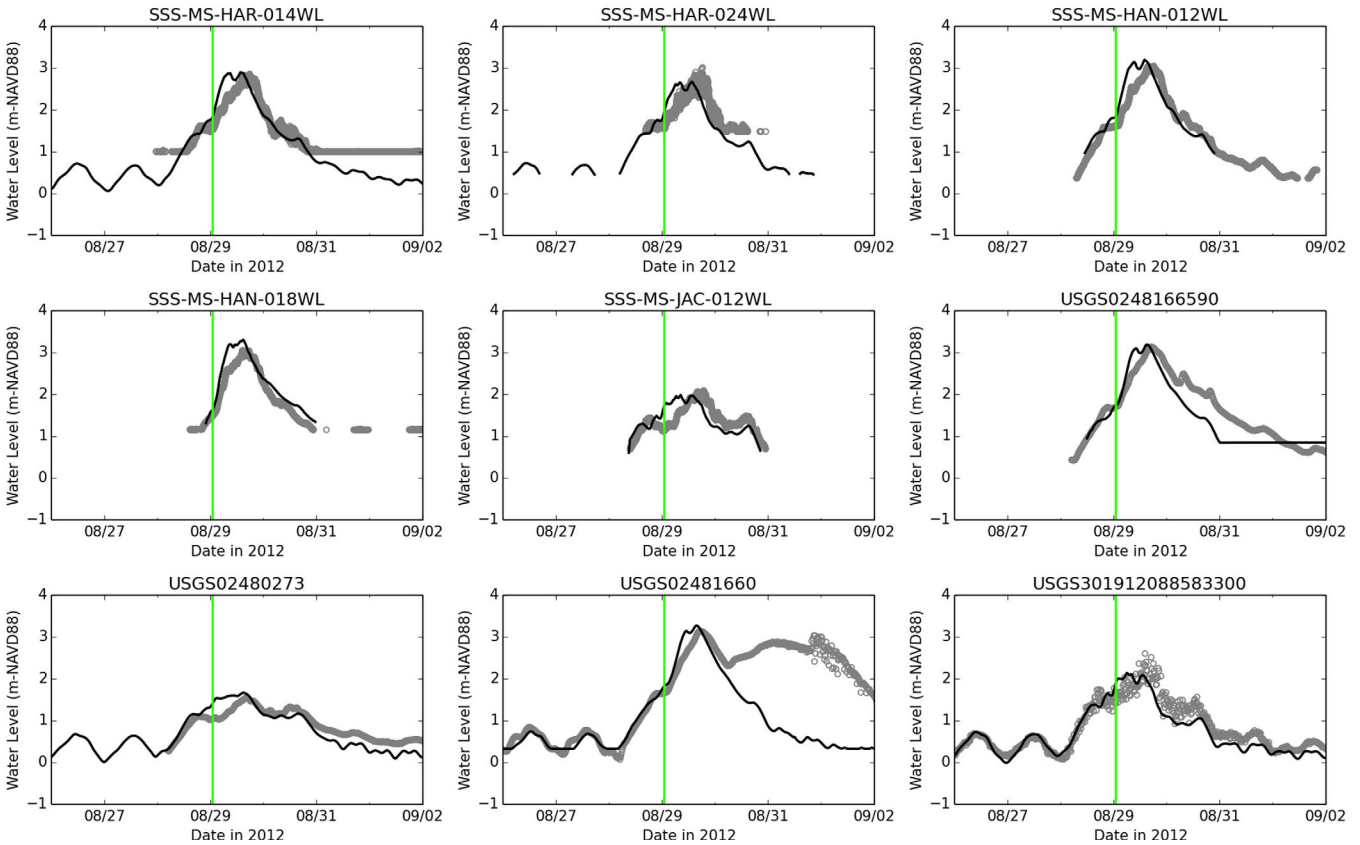

Figure 21. *NGOM3* modeled (black line) and gauge measured (gray circles) water surface elevation time series during Hurricane Isaac at a select number of stations. See File supporting information S9 for hydrographs at all stations. Landfall is represented by the green vertical line.

tide and streamgauges and supporting information File S9 shows all stations. Across all NOAA stations, the SI was 0.256 and bias is 0.043, and comparing the measured to modeled peak surge yielded an R^2 and best-fit line slope of 0.85 and 1.02, respectively (Table 3). The deployed storm tide sensors were generally located on land and this enabled validation in the accuracy of model elevations across the floodplain as well as validation of the time and elevation when wetting occurred. Across most stations, the time of simulated wetting agreed with the recorded data. For an example, see stations SSS-MS-HAN-018WL and SSS-MS-JAC-012WL (Figure 21). At all of the deployed storm tide sensors, the SI and bias were 0.195 and −0.051. Comparing peak surge at the storm tide sensors, the R^2 and slope were 0.92 and 1.05. Simulated water levels at

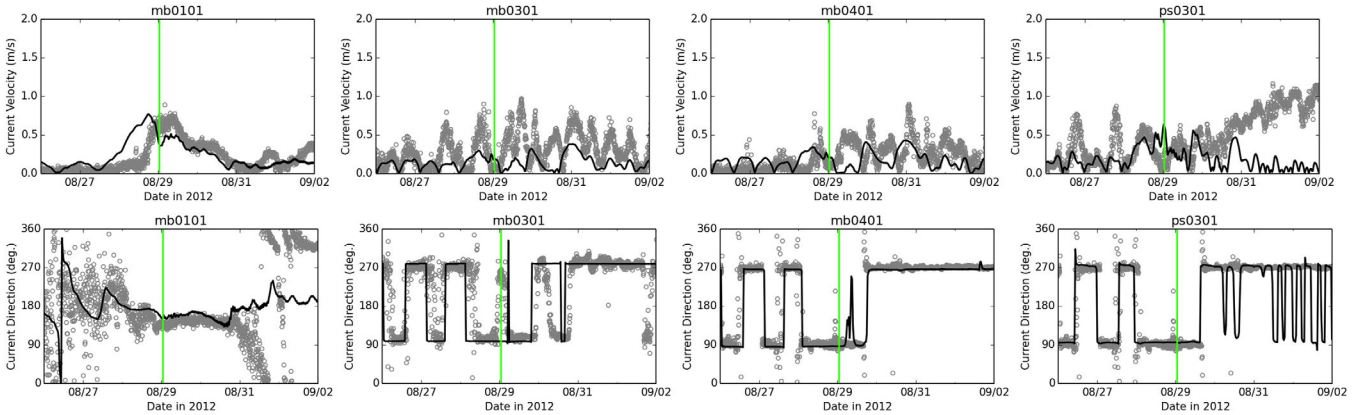

Figure 22. *NGOM3* simulated (black line) and gauge measured (gray cirlces) depth-averaged currents (m/s) and direction (deg.) during Hurricane Isaac. The vertical green line represents landfall time.

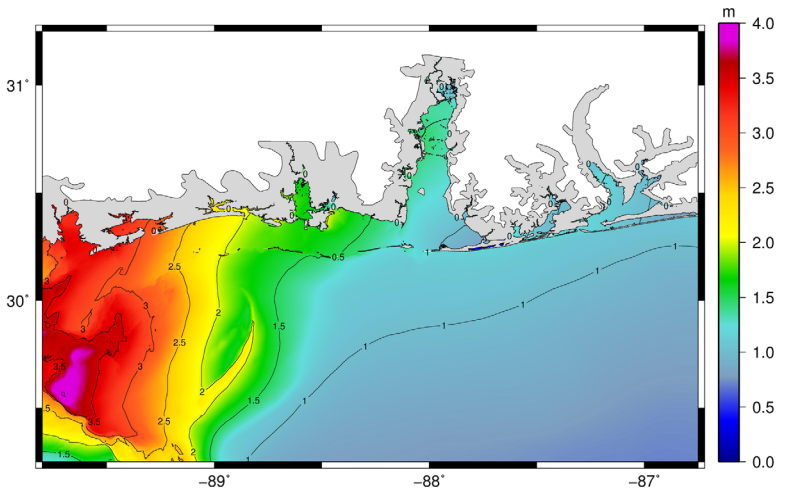

Figure 23. Maximum simulated water levels (m) across the Mississippi, Alabama, and western Florida Panhandle coast during Hurricane Isaac.

the USGS streamgauges also indicated good agreement with the measurements. The SI and bias for the permanent USGS stations were 0.264 and −0.105, and for the deployed streamgauges are 0.226 and 0.027, respectively. The streamgauges had a larger error because they are typically located upstream in small rivers or canals. Additionally, the streamgauges are affected by runoff and precipitation, which increased the post-peak water surface elevation, and was indicated by the models underprediction and the negative bias for the USGS permanent streamgauges. See USGS02481660 for an example. Among all of the locations, the SI is 0.221 and bias was −0.040.

NGOM3 simulated depth-averaged velocities during Isaac were qualitatively validated at four locations that recorded velocity magnitude and direction, two in northern Mobile Bay, one south of Dauphin Island, and one in the east Pascagoula Inlet. Figure 22 presents modeled and measured current velocity (m/s) and direction (deg.) during Isaac. The trend in *NGOM3* simulated current velocity magnitude matched well with the observed trend, considering the model did not include river flow (and the freshwater and saltwater interaction), which was the reason the model under-predicted the current velocity. All stations, except mb0101, are located at the mouth of rivers, which increased flow velocity, especially poststorm after 31 August (see ps0301). Nonetheless, the trends in the rapid increase and decrease in current magnitude were well captured in the model. Furthermore, the rapid change in direction was represented in the model, including the flood and recession of the astronomic tides, while surge is pushed north (90°) through the rivers near landfall time, and during the recession as water moved downstream (270°).

High model skill was also quantified through a HWM and gauge peaks analysis. The simulated maximum water surface elevation is presented in Figure 23. There was a total of 42 NOAA-collected HWMs in Mississippi and Alabama that were representative of stillwater elevations, and minimal effects of wave runup. A spatial map of simulated HWM error is shown in Figure 8. Of the 42 HWMs, 57% match within +/− 0.25 m and 88% match within +/- 0.5 m of the measured value. The slope of the line of best fit was 0.94 and R^2 is 0.73, and the average absolute error and the standard deviation was 0.256 and 0.284, respectively (Table 3). Including gauge peaks and HWMs, the slope of the regression line was 0.99 and R^2 is 0.85 (Figure 9). Taking into account measurement errors, the average absolute error was 0.136 and the standard deviation was 0.147 m (Table 3).

4. Summary and Conclusions

The northern GoM is a unique geophysical setting for complex tropical storm-induced hydrodynamic processes that occur across a variety of spatial and temporal scales. Each hurricane event includes its own distinctive characteristics and can cause unique and devastating storm surge when it strikes within the intricate geometric setting of the NGOM. In order to mitigate the damage and displacement from storm surge flooding, the evolution of hurricane-induced winds, waves, water levels and currents must be well

understood. In conjunction with recorded data, physics-based computer models enable researchers a comprehensive view of the deep water-, shelf- and local-scale progression of hurricane storm surge.

In this work, a numerical storm surge model for the year c. 2012 was developed using the most recent and publicly available data. The objective was to employ a single storm surge model (*i.e.* unstructured mesh, bathymetry, and surface roughness) to accurately simulate hurricane storm surge related hydrodynamics for four historical hurricanes without the need for individual model calibration. An unstructured finite element mesh was developed to describe the coastal features of the NGOM, specifically the Florida Panhandle, Alabama, and Mississippi coast. The mesh described not only the deep water and shelf-scale circulation of the GoM, but tidal flow through the wetted areas of the numerous inlet and bay systems, coastal rivers, tidal creeks, and the Gulf Intracoastal Waterway. The coastal floodplain, up to the 15 m contour, was also described with unprecedented resolution (15 m - 200 m). Named *NGOM3*, the model was employed in the tightly coupled SWAN+ADCIRC framework, forced by astronomic tides and meteorological wind and pressures. Simulated astronomic tidal constituent amplitudes and phases, in addition to a tidal resynthesis, were compared to measured tides at 43 NOAA tidal gauge stations located along the NGOM. The modeled data agreed well with the observations with *MSE/VAR* of 0.122, 0.058, and 0.085, and an RMSE of 4.698 cm, 4.377 cm, and 5.530 cm in Florida, Alabama, and Mississippi, respectively.

The evolution of simulated waves, water levels, and currents for the four hurricane events was presented and discussed and model results were validated at a variety of NDBC, NOAA, USACE, USGS, and locally operated buoys and gauge stations. In addition, poststorm collected HWM measurements were compared to the simulated maximum storm tide. Hurricane Ivan spawned a complex hydrodynamic interaction as the storm approached the nearshore. We found a minor Kelvin wave that propagated north along the WFS and triggered to an early arrival of storm surge in the *Big Bend* region of Florida, prior to landfall. South of Pensacola Bay, simulated significant wave heights of $\sim$16 m dissipated along the narrow shelf and contributed to large currents and high water levels that assisted the degradation Santa Rosa Island. The *NGOM3* simulation displayed storm surge accumulation in Chandeleur Sound, and as the storm passed, a 6 m/s outflow current was generated between the Birds Foot and storm track and was verified with ADCP observations. It was found, through numerical simulation and a comparison of observed data, that the large-scale winds dominated the local circulation; however, local water surface elevation setup can influence regional circulation through water level induced pressure gradients. A strong geostrophic current was observed across the continental shelf from a balance of the Coriolis force and the pressure gradient. The *NGOM3* simulated water levels agreed with observations with an SI and bias of 0.299 m and 0.031, respectively. It was demonstrated that the severe Ivan-induced overwash across Santa Rosa Island caused an increase in surge within Pensacola Bay and the surrounding region.

Data and simulations of Hurricane Dennis defined that a coastally trapped Kelvin Wave were generated along the WFS. The Kelvin Wave, along with locally generated wave setup, caused higher than expected storm surge in Florida's Big Bend region. The Kelvin wave propagated at a speed of 8.6 m/s, computed from the lag time via cross-correlation of the time-series water levels along the WFS. The phase speed was nearly equivalent to Dennis's forward speed (8.2 m/s). The phase speed computed from the model result compared favorably to the theoretical first-mode wave speed applied to the WFS of 8.2 m/s. Related to the coastally trapped Kelvin wave, Dennis-induced strong currents across the shelf that were oriented CCW and were in geostrophic balance with the Coriolis force and along-shelf current and water level gradients. *NGOM3* model time-series water levels agreed well to NOAA-recorded data along the west Florida coast as well as to analytical solutions of the magnitude and cross-shelf width of the coastally trapped wave. At the measured HWMs, simulated maximum storm tide matched within +/- 0.25 m at 55% and was within +/− 0.5 m at 99% of the 142 measured locations; additionally, the line of best fit had a slope of 0.93, the R^2 was 0.73.

Hurricane Katrina generated record-breaking significant wave heights of nearly 17 m in the GoM and over 8 m of maximum water levels along the Mississippi Coast. Through an assessment of data and the *NGOM3* model results it was observed that Katrina excited a CTW with a phase speed of 11 m/s along the WFS and 12.2 m/s across the shelf south of the Florida Panhandle. The CTW caused currents to shift in a CCW fashion prior to the local changes in the wind direction, which suggests that the large-scale wind fields dominate the regional and local circulation patterns. In terms of coastal flooding, it was shown that the majority of inundation along the Mississippi coast occurred within 6 hr. Pass Christian was flooded from both the north

along the south shore of the Bay of St. Louis and from the GoM shore to the south. Strong south-southeasterly winds pushed water up the Pascagoula River and adjacent marsh and piled up against US90. Surge moved into Mobile Bay from the west, and locally generated wind setup continued to move water into the northern portions of Mobile Bay and created 2 m of surge along the western Florida Panhandle coast. Comparing recorded and simulated time-series water levels at 32 stations across the NGOM yielded an SI and normalized bias of 0.212 and −0.009, respectively. Comparing HWMs and gauge peaks yielded an average absolute error of 0.089 m and 0.140, respectively. The slope of the line of best fit was 1.00 with an R^2 of 0.97.

The synoptic analysis of the simulated evolution of Hurricane Isaac, yet again, unveiled that a CTW was induced and propagate along the WFS at a speed of 14 m/s – 17 m/s across the WFS and 6.5 m/s across the shelf from Apalachicola to Pensacola. The CTW caused surge of near 1.5 in Florida's Big Bend region prior to landfall in Louisiana. Strong along-shelf currents persisted in a CCW orientation and caused surge to build up along the eastern Mississippi River and in the Biloxi marsh. Similar to Hurricane Ivan, a strong outflow current was present east of the Birds Foot along the shelf break. A maximum simulated storm tide of ∼3.5 occurred in the back of the Bay of St. Louis. The simulated processes were validated when results were compared to data at 81 gauges that recorded time-series water levels where the SI and bias were 0.221 m and −0.040, and the average absolute error at 110 HWMs and gauge peaks was 0.136 m.

This work presents the most in-depth synoptic analysis and validation in the literature of Hurricanes Ivan and Dennis across the NGOM and Hurricane Katrina within Mississippi and specifically Alabama and the western Florida Panhandle. Additionally, this is the first work analyzing and validating Hurricane Isaac, particularly for the NGOM region. From the analysis of the *NGOM3* simulations, we determine that the large-scale winds play a dominant role in the large-scale and local circulation, especially across the continental shelf. The strong currents were caused by the hurricane-induced geostrophic balance with the Coriolis force and water level pressure gradients. Most hurricanes that track into the GoM will excite a CTW that propagates along the WFS and induces an early arrival of storm surge in the *Big Bend* region. The model results are trusted based on the qualitative and quantitative measures among the astronomic tide and four hurricane storm surge simulations, which indicate a well-performing model. Not only did the model agree with a variety of recorded data, but results also agreed with analytical solutions of shelf and local scale processes. This work proves that a single high-resolution two-dimensional physics-based storm surge model can be developed and applied to a variety of forcing criteria and yield accurate results without the need for individual event model calibration. This is advantageous when hurricane characteristics are not known *a priori*, such as estimating storm surge in a real-time forecasting system or estimating future coastal flood risk under global climate change and sea level rise in particular.

Acknowledgments

This research was funded in part under award NA10NOS4780146 from the National Oceanic and Atmospheric Administration (NOAA) Center for Sponsored Coastal Ocean Research (CSCOR), award NFWMD-08-073 from the Northwest Florida Water Management District (NWFWMD), and the Louisiana Sea Grant Laborde Chair. This work used the Extreme Science and Engineering Discovery Environment (XSEDE), which is supported by the National Science Foundation (NSF) grant ACI-1053575 [*Towns et al.*, 2014]. This work also used High-Performance Computing at Louisiana State University (LSU) and the Louisiana Optical Network Initiative (LONI). Supporting data are included in the SI files. We thank our colleagues J. H. Atkinson, Z. Cobell, J. C. Dietrich, and H. J. Roberts who provided expertise that greatly assisted this research, D. Justic for performing an internal review of the manuscript, and the anonymous reviewers for their insightful comments that drastically improved the manuscript. The statements and conclusions are those of the authors and do not necessarily reflect the views of NOAA, NWFWMD, Louisiana Sea Grant, XSEDE, NSF, LSU, or LONI.

References

Atkinson, J. H., H. J. Roberts, S. C. Hagen, S. Zou, P. Bacopoulos, S. C. Medeiros, J. F. Weishampel, and Z. Cobell (2011), Deriving frictional parameters and performing historical validation for an ADCIRC storm surge model of the Florida Gulf Coast, *Florida Watershed J.*, *4*(2), 22–27.

Bacopoulos, P., D. M. Parrish, and S. C. Hagen (2011), Unstructured mesh assessment for tidal model of the South Atlantic Bight and its estuaries, *J. Hydraul. Eng.*, *49*(4), 487–502.

Bacopoulos, P., B. R. Dally, S. C. Hagen, and A. T. Cox (2012), Observations and simulation of winds, surge, and currents on Florida's east coast during hurricane Jeanne (2004), *Coastal Eng.*, *60*, 84–94.

Battjes, J. A., and J. P. F. M. Janssen (1978), Energy loss and set-up due to breaking of random waves, paper presented at the ASCE, Proceedings of the 16th Conference on Coastal Engineering, Hamburg, Germany.

Berg, R. (2012), Hurricane Isaac, report, Natl. Oceanic and Atmos. Admin., Natl. Weather Serv., Trop. Predict. Cent., Miami, Fla.

Beven, J. (2005), Hurricane Dennis, report, Natl. Oceanic and Atmos. Admin., Natl. Weather Serv., Trop. Predict. Cent., Miami, Fla.

Bilskie, M. V., S. C. Hagen, S. C. Medeiros, and D. L. Passeri (2014), Dynamics of sea level rise and coastal flooding on a changing landscape, *Geophys. Res. Lett.*, *41*, 927–934, doi:10.1002/2013GL058759.

Bilskie, M. V., D. Coggin, S. C. Hagen, and S. C. Medeiros (2015), Terrain-driven unstructured mesh development through semi-automatic vertical feature extraction, *Adv. Water Resour.*, vol. 86(Part A), pp. 102–118.

Black, P. G., E. A. D'Asaro, T. B. Sanford, W. M. Drennan, J. A. Zhang, J. R. French, P. P. Niiler, E. J. Terrill, and E. J. Walsh (2007), Air–sea exchange in hurricanes: Synthesis of observations from the coupled boundary layer air–sea transfer experiment, *Bull. Am. Meteorol. Soc.*, *88*(3), 357–374.

Booij, N., R. C. Ris, and L. H. Holthuijsen (1999), A third-generation wave model for coastal regions 1. Model description and validation, *J. Geophys. Res.*, *104*(C4), 7649–7666.

Buczkowski, B. J., J. A. Reid, J. A. Jenkins, C. J. Reid, S. J. Williams, and J. G. Flocks (2006), usSEABED: Gulf of Mexico and Caribbean (Puerto Rico and U.S. Virigin Islands) offshore surficial sediment data release, U.S. Geol. Surv. Data Ser. 146, version 1.0, Reston, Va.

Bunya, S., et al. (2010), A high-resolution coupled riverine flow, tide, wind, wind wave, and storm surge model for southeastern Louisiana and Mississippi. Part I: Model development and validation, *Mon. Weather Rev.*, 128(345-377).

Cavaleri, L., and P. M. Rizzoli (1981), Wind wave prediction in shallow water: Theory and applications, *J. Geophys. Res.*, *86*(C11), 10,961–10,973.
Chen, C., H. Liu, and R. C. Beardsley (2003), An unstructured grid, finite-volume, three-dimensional, primitive equations ocean model: Application to coastal ocean and estuaries, *J. Atmos. Oceanic Technol.*, *20*(1), 159–186.
Chen, Q., L. Wang, and R. Tawes (2008), Hydrodynamic response of Northeastern Gulf of Mexico to hurricanes, *Estuaries Coasts*, *31*(6), 1098–1116.
Chow, V. T. (1959), *Open-Channel Hydraulics*, McGraw-Hill, N. Y.
Clarke, A. J. (1977), Observational and numerical evidence for wind-forced coastal trapped long waves, *J. Phys. Oceanogr.*, *7*(2), 231–247.
Clarke, A. J., and S. Van Gorder (1986), A method for estimating wind-driven frictional, time-dependent, stratified shelf and slope water flow, *J. Phys. Oceanogr.*, *16*(6), 1013–1028.
Claudino-Sales, V., P. Wang, and M. H. Horwitz (2010), Effect of hurricane Ivan on Coastal Dunes of Santa Rosa Barrier Island, Florida: Characterized on the basis of pre- and poststorm LIDAR surveys, *J. Coastal Res.*, *26*(3), pp. 470–484.
Coggin, D., S. C. Hagen, and M. B. Salisbury (2011), A digital elevation model for Franklin, Wakulla, and Jefferson Counties, *Florida Watershed J.*, *4*(2), 5–10.
Cox, A. T., J. A. Greenwood, V. J. Cardone, and V. R. Swail (Eds.) (1995), *An Interactive Objective Kinematic Analysis System*, 4th International Workshop on Wave Hindcasting and Forecasting, Banff, Alberta.
Dietrich, J. C., M. Zijlema, J. J. Westerink, L. H. Holthuijsen, C. N. Dawson, R. A. Luettich, R. E. Jensen, J. M. Smith, G. S. Stelling, and G. W. Stone (2011a), Modeling hurricane waves and storm surge using integrally-coupled, scalable computations, *Coastal Eng.*, *58*, 45–65.
Dietrich, J. C., et al. (2011b), Hurricane Gustav (2008) waves and storm surge: Hindcast, synoptic analysis, and validation in southern Louisiana, *Mon. Weather Rev.*, *139*(8), 2488–2522.
Dietrich, J. C., S. Tanaka, J. J. Westerink, C. N. Dawson, R. A. Luettich, M. Zijlema, L. H. Holthuijsen, J. M. Smith, L. G. Westerink, and H. J. Westerink (2012), Performance of the Unstructured-Mesh, SWAN+ADCIRC Model in Computing Hurricane Waves and Surge, *J. Sci. Comput.*, *52*(2), 468–497.
Dietrich, J. C., et al. (2013), Limiters for spectral propagation velocities in SWAN, *Ocean Modell.*, *70*, 85–102.
Ding, Y., S. Nath Kuiry, M. Elgohry, Y. Jia, M. S. Altinakar, and K.-C. Yeh (2013), Impact assessment of sea-level rise and hazardous storms on coasts and estuaries using integrated processes model, *Ocean Eng.*, *71*, 74–95.
Donnelly, C., N. C. Karaus, and M. larson (2004), Coastal overwash. Part 1, Report no. ERDC/RSM-TN-14, 36 pp., US Army Eng. Res. and Dev. Cent., Vickburg, Miss.
Dukhovskoy, D., and S. Morey (2011), Simulation of the Hurricane Dennis storm surge and considerations for vertical resolution, *Nat. Hazards*, *58*(1), 511–540.
Ebersole, B. A., J. J. Westerink, S. Bunya, J. C. Dietrich, and M. A. Cialone (2010), Development of storm surge which led to flooding in St. Bernard Polder during Hurricane Katrina, *Ocean Eng.*, *37*(1), 91–103.
Egbert, G. D., and S. Y. Erofeeva (2002), Efficient inverse modeling of barotropic ocean tides, *J. Atmos. Oceanic Technol.*, *19*(2), 183–204.
Egbert, G. D., A. F. Bennett, and M. G. G. Foreman (1994), TOPEX/POSEIDON tides estimated using a global inverse model, *J. Geophys. Res.*, *99*(C12), 24,821-24,852.
Freeman, J. C., L. Baer, and G. H. Jung (1957), The bathystrophic storm tide, *J. Mar. Res.*, *16*(1), 12–22.
Garratt, J. R. (1977), Review of drag coefficients over oceans and continents, *Mon. Weather Rev.*, *105*(7), 915–929.
Gore, R. H. (1992), *The Gulf of Mexico: A Treasury of Resources in the American Mediterranean*, Pineapple Press, Sarasota, Fla.
Gouillon, F., S. L. Morey, D. S. Dukhovskoy, and J. J. O'Brien (2010), Forced tidal response in the Gulf of Mexico, *J. Geophys. Res.*, *115*, C10050, doi:10.1029/2010JC006122.
Hagen, S. C., and D. M. Parrish (2004), Meshing requirements for tidal modeling in the western North Atlantic, *Int. J. Comput. Fluid Dyn.*, *18*(7), 585–595.
Hagen, S. C., J. J. Westerink, and R. L. Kolar (2000), One-dimensional finite element grids based on a localized truncation error analysis, *Int. J. Numer. Methods Fluids*, *32*(2), 241–262.
Hagen, S. C., J. J. Westerink, R. L. Kolar, and O. Horstmann (2001), Two-dimensional, unstructured mesh generation for tidal models, *Int, J, Numer, Methods Fluids*, *35*, 669–686.
Hagen, S. C., P. Bacopoulos, S. C. Medeiros, D. Coggin, M. B. Salisbury, J. H. Atkinson, and H. J. Roberts (2009), Storm surge modeling for FEMA map modernization for Franklin, Wakulla, and Jefferson Counties, Florida, report, Univ. of Central Fla.
Hagen, S. C., P. Bacopoulos, A. T. Cox, and V. J. Cardone (2011), Hydrodynamics of the 2004 Florida Hurricanes, *J. Coastal Res.*, *28*(5), 1121–1129.
Holland, K., R. A. Holman, and A. Sallenger (1991), Estimation of overwash bore velocities using video techniques, paper presented at Coastal Sediments '91, Am. Soc. of Civ. Eng., pp. 489–497, Seattle, Wash.
Holthuijsen, L. H. (2007), *Waves in Oceanic and Coastal Waters*, xvi, 387 pp., Cambridge Univ. Press, Cambridge, U. K.
Hope, M. E., et al. (2013), Hindcast and validation of Hurricane Ike (2008) waves, forerunner, and storm surge, *J. Geophys. Res. Oceans*, *118*, 4424–4460, doi:10.1002/jgrc.20314.
Hu, C., and F. E. Muller-Karger (2007), Response of sea surface properties to Hurricane Dennis in the eastern Gulf of Mexico, *Geophys. Res. Lett.*, *34*, L07606, doi:10.1029/2006GL028935.
Kennedy, A. B., U. Gravois, B. C. Zachry, J. J. Westerink, M. E. Hope, R. A. Luettich, and R. G. Dean (2011), Origin of the Hurricane Ike forerunner surge, *Geophys. Res. Lett.*, *38*, L08608, doi:10.1029/2011GL047090.
Kim, K., H. Lee, T. Yamashita, and B. Choi (2008), Wave and storm surge simulations for Hurricane Katrina using coupled process based models, *KSCE J. Civ. Eng.*, *12*(1), 1–8.
Knabb, R. D., J. R. Rhome, and D. P. Brown (2005), Hurricane Katrina, report, Natl. Oceanic and Atmos. Admin., Natl. Weather Serv., Trop. Predict. Cent., Miami, Fla.
Kolar, R. L., W. Grey, J. J. Westerink, and R. A. Luettich (1994), Shallow water modeling in spherical coordinates: Equation formulation, numerical implementation, and application, *J. Hydraul. Res.*, *32*(1), 3–24.
Komen, G. J., K. Hasselmann, and K. Hasselmann (1984), On the Existence of a Fully Developed Wind-Sea Spectrum, *J. Phys. Oceanogr.*, *14*(8), 1271–1285.
Kraft, B. J., and C. de Moustier (2010), Detailed bathymetric surveys offshore Santa Rosa Island, FL: Before and after Hurricane Ivan (September 16, 2004), *IEEE J. Oceanic Eng.*, *35*(3), 453–470.
Le, L. (1994), A numerical study of sea level and current responses to Hurricane Frederic using a coastal ocean model for the Gulf of Mexico, *J. Oceanogr.*, *50*(6), 599–616.
Luettich, R. A., and H. J. Westerink (2000), ADCIRC: A (Parallel) advanced circulation model for oceanic, coastal, and estuarine waters, report, 115 pp. [Available at http://www3.nd.edu/adcirc/manual/ADCIRC_manual.pdf.]

Luettich, R. A., and J. J. Westerink (2004), Formulation and numerical implementations of the 2D/3D ADCIRC finite element model version 44.XX. [Available at https://www.researchgate.net/publication/240474926Formulation_and_Numerical_Implementation_of_the_2D3D_ADCIRC_Finite_Element_Model_Version_44.]

Luettich, R. A., J. J. Westerink, and N. W. Scheffner (1992), ADCIRC: An advanced three-dimensional circulation model for shelves, coasts, and estuaries, I: Theory and methodology of ADCIRC-2DDI and ADCIRC-3DL, Dredging Research Program Technical Report DRP-92-6, 137 pp., U.S. Army Engineers Waterways Experiment Station, Vicksburg, Miss.

Luther, M. E., C. R. Merz, J. Scudder, S. R. Baig, J. L. T. Pralgo, D. Thompson, S. Gill, and G. Hovis (2007), Water level observations for storm surge, *Mar. Technol. Soc. J.*, *41*(1), 35–43.

Madsen, O. S., Y. K. Poon, and H. C. Graber (1988), *Spectral Wave Attenuation By Bottom Friction: Theory*, Presented at the 21st International Conference on Coastal Engineering, Amer. Soc. of Civil Eng., 3040 pp., 3 vols, Torremolinos, Spain.

Martyr, R. C., et al. (2013), Simulating hurricane storm surge in the lower Mississippi River under varying flow conditions, *J. Hydraul. Eng.*, *139*(492), 492–501.

McCall, R. T., J. S. M. Van Thiel de Vries, N. G. Plant, A. R. Van Dongeren, J. A. Roelvink, D. M. Thompson, and A. J. H. M. Reniers (2010), Two-dimensional time dependent hurricane overwash and erosion modeling at Santa Rosa Island, *Coastal Eng.*, *57*(7), 668–683.

McCallum, B. E., B. D. McGee, D. R. Kimbrow, M. S. Runner, J. A. Painter, E. R. Frantz, and A. J. Gotvald (2012), Monitoring storm tide and flooding from Hurricane Isaac along the Gulf Coast of the United States, U.S. Geological Survey Open-File Report 2012–1263, 24 pp., Reston, Va. [Available online at http://pubs.usgs.gov/of/2012/1263/.]

Medeiros, S. C., T. Ali, and S. C. Hagen (2011), Development of a seamless topographic/bathymetric digital terrain model for Tampa Bay, Florida, *Photogramm. Eng. Remote Sens.*, *77*(12), 1249–1256.

Mitchell, D. A., W. J. Teague, E. Jarosz, and D. W. Wang (2005), Observed currents over the outer continental shelf during Hurricane Ivan, *Geophys. Res. Lett.*, *32*, L11610, doi:10.1029/2005GL023014.

Mitchum, G. T., and A. J. Clarke (1986), Evaluation of frictional, wind-forced long-wave theory on the West Florida Shelf, *J. Phys. Oceanogr.*, *16*(6), 1029–1037.

Mitchum, G. T., and W. Sturges (1982), Wind-driven currents on the West Florida Shelf, *J. Phys. Oceanogr.*, *12*(11), 1310–1317.

Morey, S. L., S. Baig, M. A. Bourassa, D. S. Dukhovskoy, and J. J. O'Brien (2006), Remote forcing contribution to storm-induced sea level rise during Hurricane Dennis, *Geophys. Res. Lett.*, *33*, L19603, doi:10.1029/2006GL027021.

Pedlosky, J. (1992), *Geophysical Fluid Dynamics*, 2nd ed., Springer, N. Y.

Powell, M. D. (2006), Drag coefficient distribution and wind speed dependence in tropical cyclones, Final report to the National Oceanic and Atmospheric Administration (NOAA) Joint Hurricane Testbed (JHT) program, Tech. Rep., Atlantic Oceanogr. and Meteorol. Lab., Miami, Fla. [Available at http://www.nhc.noaa.gov/jht/05-07reports/final_Powell_JHT07.pdf.]

Powell, M. D., S. H. Houston, L. R. Amar, and N. L. Morisseau-Leroy (1998), The HRD real-time hurricane wind analysis system, *J. Wind Eng. Ind. Aerodyn.*, *77–78*, pp. 53–64.

Powell, M. D., P. J. Vickery, and T. A. Reinhold (2003), Reduced drag coefficient for high wind speeds in tropical cyclones, *Nature*, *422*, 279–283.

Powell, M. D., et al. (2010), Reconstruction of Hurricane Katrina's wind fields for storm surge and wave hindcasting, *Ocean Eng.*, *37*, 26-26.

Resio, D. T., and J. J. Westerink (2008), Modeling the physics of storm surges, *Phys. Today*, *61*(9), 33–38.

Rogers, W. E., P. A. Hwang, and D. W. Wang (2003), Investigation of wave growth and decay in the SWAN Model: Three regional-scale applications*, *J. Phys. Oceanogr.*, *33*(2), 366–389.

Salisbury, M. B., and S. C. Hagen (2007), The effect of tidal inlets on open coast storm surge hydrographs, *Coastal Eng.*, *54*(5), 377–391.

Salisbury, M. B., S. C. Hagen, D. Coggin, P. Bacopoulos, J. H. Atkinson, and H. J. Roberts (2011), Unstructured mesh development for the Big Bend Region (Florida), *Florida Watershed J.*, *4*(2), 11–14.

Sallenger, A. H., Jr. (2000), Storm impact scale for Barrier Islands, *J. Coastal Res.*, *16*(3), 890–895.

Sheng, Y. P., Y. Zhang, and V. A. Paramygin (2010), Simulation of storm surge, wave, and coastal inundation in the Northeastern Gulf of Mexico region during Hurricane Ivan in 2004, *Ocean Modell.*, *35*(4), 314–331.

Stewart, S. R. (2004), Hurricane Ivan, report, Natl. Oceanic and Atmos. Admin., Natl. Weather Serv., Trop. Predict. Cent., Miami, Fla.

Stone, G. W., N. D. Walker, A. Hsu, A. Babin, B. Liu, B. D. Keim, W. Teague, D. Mitchell, and R. Leben (2005), Hurricane Ivan's impact along the northern Gulf Of Mexico, *Eos Trans. AGU*, *86*(48), 497–501.

Sullivan, P. P., L. Romero, J. C. McWilliams, and W. K. Melville (2012), Transient evolution of Langmuir turbulence in ocean boundary layers driven by hurricane winds and waves, *J. Phys. Oceanogr.*, *42*(11), 1959–1980.

Teague, W. J., E. Jarosz, D. W. Wang, and D. A. Mitchell (2007), Observed oceanic response over the upper continental slope and outer shelf during Hurricane Ivan*, *J. Phys. Oceanogr.*, *37*(9), 2181–2206.

Thompson, E., and V. Cardone (1996), Practical modeling of hurricane surface wind fields, *J. Waterw. Port Coastal Ocean Eng.*, *122*(4), 195–205.

Towns, J., et al. (2014), XSEDE: Accelerating scientific discovery, *IEEE Comput. Sci. Eng.*, *16*(5), 62–74.

University of Central Florida (2011a), Digital elevation model and finite element mesh development, report, Northwest Fla. Water Manage. District and the Fed. Emergency Manage. Agency, Orlando.

University of Central Florida (2011b), Flood insurance study: Florida Panhandle and Alabama, Model Validation, report, Fed. Emergency Manage. Agency.

Wang, B. (2003), Kelvin Waves, in *Encyclopedia of Meteorology*, edited by J. Holton, pp. 1062–1068, Academic Press, Oxford, U. K.

Wang, D. W., D. A. Mitchell, W. J. Teague, E. Jarosz, and M. S. Hulbert (2005), Extreme Waves Under Hurricane Ivan, *Science*, *309*(5736), 896.

Weisberg, R. H., and R. He (2003), Local and deep-ocean forcing contributions to anomalous water properties on the West Florida Shelf, *J. Geophys. Res.*, *108*(C6), 3184, doi:10.1029/2002JC001407.

Weisberg, R. H., and L. Zheng (2008), Hurricane storm surge simulations comparing three-dimensional with two-dimensional formulations based on an Ivan-like storm over the Tampa Bay, Florida region, *J. Geophys. Res.*, *113*, C12001, doi:10.1029/2008JC005115.

Yang, Z., T. Wang, R. Leung, K. Hibbard, T. Janetos, I. Kraucunas, J. Rice, B. Preston, and T. Wilbanks (2014), A modeling study of coastal inundation induced by storm surge, sea-level rise, and subsidence in the Gulf of Mexico, *Nat. Hazards*, *71*(3), 1771–1794.

Zijlema, M. (2010), Computation of wind-wave spectra in coastal waters with SWAN on unstructured grids, *Coastal Eng.*, *57*(3), 267–277.